NASA
Technical
Paper
2286
C.2
March 1984

Overview of Zirconia With Respect to Gas Turbine Applications

James D. Cawley

NASA

NASA Technical Paper 2286

1984

Overview of Zirconia With Respect to Gas Turbine Applications

James D. Cawley

Lewis Research Center
Cleveland, Ohio

National Aeronautics and Space Administration

Scientific and Technical Information Branch

Summary

The literature on zirconia is reviewed, with an emphasis on material properties, referenced to its application in gas turbine engines. The review indicates that Mg-PSZ (partially stabilized zirconia) and Ca-PSZ are unsuitable for advanced gas turbine applications; a thorough characterization of the microstructure of plasma-sprayed zirconia is needed. Transformation-toughened zirconia may be suitable for use in monolithic components.

Introduction

Zirconia is a material with interesting and unique properties. Many varied applications take advantage of these properties. Its high melting point, 2680° C, low thermal conductivity, and relatively high resistance to chemical attack have made zirconia an attractive refractory material. Furnaces are available with zirconia insulation; it is also used for heating elements either as a susceptor in an induction furnace or as Joule-effect heating elements (ref. 1). Although it is necessary to preheat the zirconia to ~1000° C before it will become sufficiently conductive, it does provide a material for resistance heating elements, which are used to obtain very high temperatures in an oxidizing atmosphere. Other refractory applications include refractory bricks for magnetohydrodynamics (MHD) and magnetogasdynamics (MGD) (ref. 1). The high levels of ionic conductivity of stabilized zirconia alloys (most often stabilized with Ca or Y) have led to their use as oxygen sensors (ref. 1) and in fuel cells (ref. 2). The high index of refraction of single crystals of fully stabilized cubic zirconia, which is very similar to that of diamond, makes them a source for synthetic jewels (ref. 3). The natural abundance of zirconia in the Earth's crust is reported to be 0.02 to 0.03 percent (ref. 3), which is enough to sustain this wide range of applications.

In the hot section of gas turbine engines there are three main areas of interest and application for zirconia: as a combustor can liner (ref. 4), as a thermal barrier coating for turbine hardware (ref. 5), and as turbine blade tip-gas path seals (ref. 6). Each application has particular requirements. For example, in the combustor liner it is desirable to raise the wall temperature while lowering the underlying metal temperature (ref. 7). The thermal barrier coating on turbine hardware imposes an aerodynamic drag that must be eliminated by finishing the surface (ref. 8). The gas path seal has the contradictory requirements of abradability (during a turbine blade tip-seal rub the seal should preferentially wear) while having a high erosion resistance (to prevent the particulates in the gas from wearing the seal and opening up the clearance) (ref. 6). All of these applications, however, have a great deal in common. They all see a cyclic thermal environment, they all are subjected to hot corrosive gases, and they all involve a metal-ceramic bond (since they are currently fabricated by plasma spraying (ref. 9) the zirconia to a metal part).

The success of these applications depends on the material properties of zirconia (e.g., the thermal expansion, the Young's and shear moduli, the fracture toughness, the thermal conductivity, and the plastic deformation). The effects of plasma spraying and postfabrication alteration of the material, either intentional or during use, on these properties are critical to the success or failure of their application. These properties and effects also must be known to simulate and analytically predict some aspects of turbine blade tip-seal behavior.

This document is a compilation of information, gathered from the literature, on the properties of zirconia. Although the importance of the bond coat is recognized, it will be dealt with only peripherally. The motivation for this work lies in the author's interest in abradable turbine blade tip-gas path seals. However, the information is felt to be general to all gas turbine applications. The document is divided into five sections:

(1) Phase relationships and mechanical properties
(2) Thermal conductivity
(3) Deformation
(4) Diffusion
(5) Chemical reactivity

Each section consists of an introduction to the subject, a review of the observations on zirconia, observations particular to plasma-sprayed material, and implications for gas turbine applications. Both criticism and suggestions are offered.

Phase Relationships and Mechanical Properties

Phase Relationships in Pure Zirconia

The range of application of pure zirconia (ZrO_2) is greatly limited by two solid-state phase transitions and the attendant volume changes. The phase relationships are described by (ref. 3)

$$\text{Monoclinic} \underset{}{\overset{1170^\circ\text{ C}}{\rightleftharpoons}} \text{Tetragonal} \overset{2370^\circ\text{ C}}{\rightleftharpoons} \text{Cubic} \overset{2680^\circ\text{ C}}{\rightleftharpoons} \text{Liquid}$$

The high-temperature cubic phase can be further specified as the fluorite structure. In this structure the anion (oxygen) sublattice is simple cubic and the cation (zirconium) sublattice is face-centered cubic. The two sublattices are combined such that the cations occupy every other eightfold coordinated site in the anion sublattice; this is illustrated in figure 1.

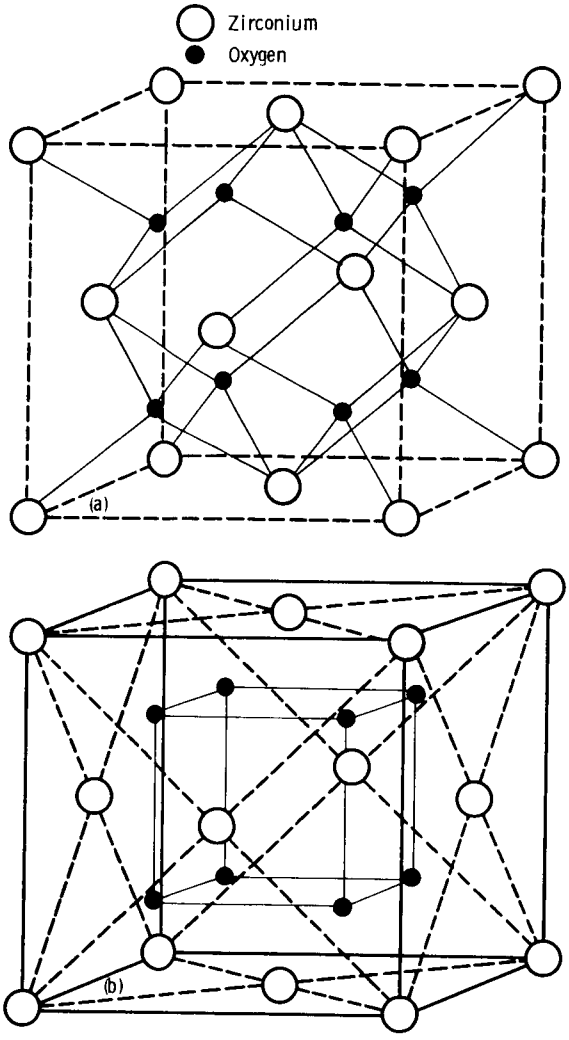

(a) Fluorite structure showing the eightfold coordination of the zirconium.
(b) Fluorite structure highlighting the simple cubic oxygen sublattice and the face-centered cubic zirconium sublattice.

Figure 1. – Oxygen and zirconium sublattices.

As the material is cooled past 2370° C, a transition to a tetragonal structure takes place. Although the mechanism of this transition is not well understood (ref. 3) because of the difficulty of making observations at such a high temperature, it is presumed that this tetragonal form is a distorted fluorite structure.

The face-centered tetragonal unit cell commonly (although not exclusively) used in describing the tetragonal phase is not a primitive cell; that is, there exists a body-centered tetragonal unit cell that contains fewer lattice sites. The relationship between the two cells is illustrated in figure 2. The reason for this choice is to preserve the analogy between the cubic and tetragonal forms.

As the material is further cooled past 1170° C, it undergoes a martensitic transformation (the significance of which will be returned to) to monoclinic symmetry

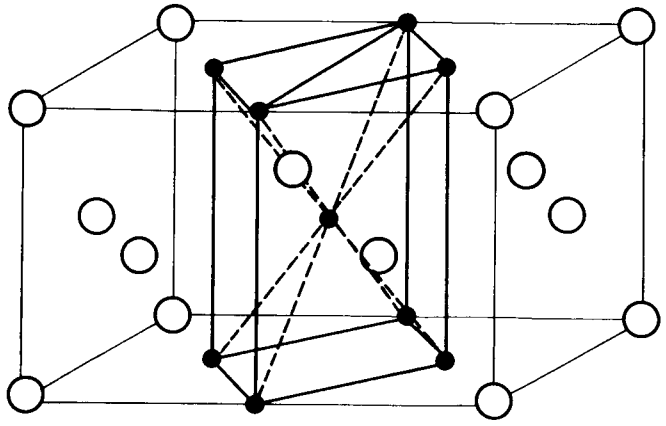

Figure 2. – Two face-centered tetragonal unit cells with body-centered tetragonal cell shown by the heavy lines.

(fig. 3). This is a disruptive transformation in which the coordination number of zirconium drops to 7 (ref. 10) and causes pieces of the material to break into powder from internal stresses.

The lattice parameters (the room-temperature cubic lattice parameters are an extrapolation) and the unit cell volumes are given in table I and illustrated in figure 4. The transition from cubic to tetragonal involves a small strain, 0.1 percent, and this occurs at high temperatures, where the resultant stresses may presumably be readily relieved. On the other hand, the tetragonal-to-monoclinic transformation involves a strain of ~ 1.5 percent and occurs below the ductile-to-brittle transition for ZrO_2. McCartney et al. (ref. 11) found that the ductile-to-brittle transition for Ca-SZ occurs between 1200° and 1350° C at a strain rate of 1×10^{-4} sec^{-1}.

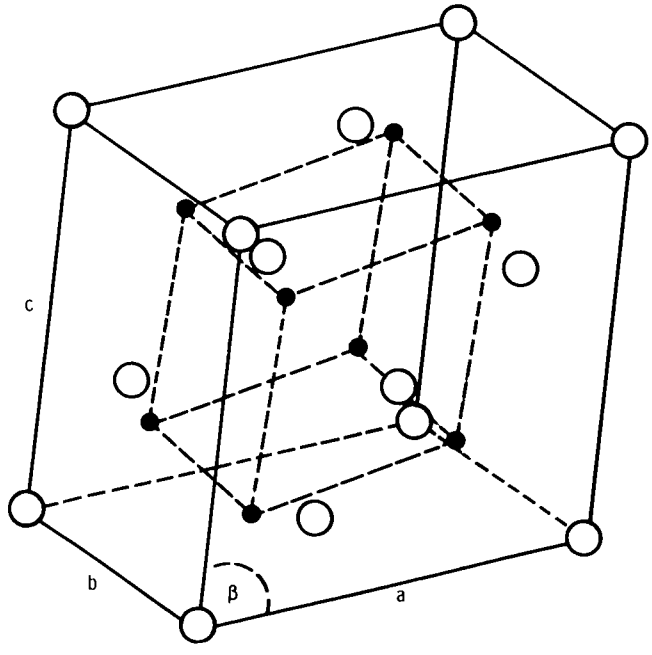

Figure 3. – Monoclinic structure of zirconia. (From ref. 80.)

TABLE I. – LATTICE PARAMETERS AND UNIT CELL VOLUMES

Phase	Lattice parameter, nm				Unit cell volume	Reference
	a	b	c	β		
Cubic	0.5113	-----	-----	-----	1.3367×10^2	36
Tetragonal	.5082	-----	0.5185	-----	1.3391×10^2	36
Monoclinic	.5147	0.5206	.5135	8.077	1.358×10^2	79

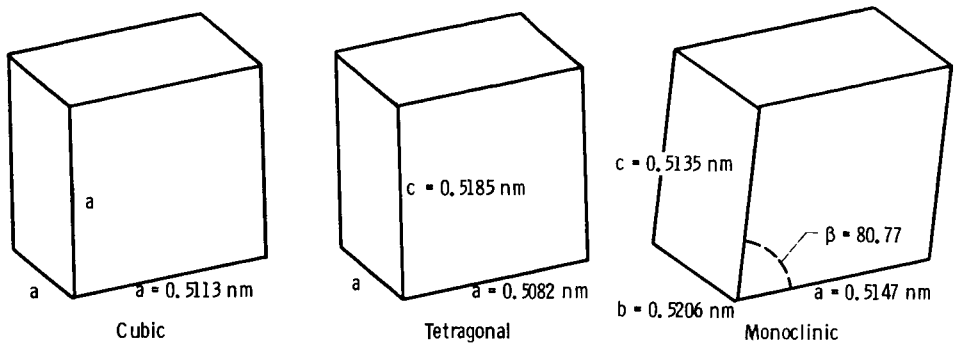

Figure 4. – Schematic of three polymorphs of zirconia.

Stabilization of Zirconia

It has been known for more than 50 years (ref. 25) that the alloying of ZrO_2 with particular oxides produces a stabilized system; that is, the phase transitions can be avoided and the material will remain cubic at all temperatures. These systems, as pointed out by Heuer (ref. 25), are not truly stable. The single-phase behavior results from the depression of the phase transition temperature to a value low enough that the reaction kinetics are essentially zero.

A large number of stabilizers have been investigated, most successfully with the alkaline earths and rare earths; those that have received much attention are Mg, Ca, and Y. In addition, there is some indication that the use of other stabilizers, such as CeO_2 (ref. 12), that give a low thermal expansion may have other advantages. Material that is fully stabilized has a larger thermal expansion coefficient than pure ZrO_2 (fig. 5). Therefore, despite the absence of phase transitions, its use may be limited by its response to thermal gradients. It is now well documented (refs. 13 to 15) that the best engineering properties can be obtained by using a multiphase, partially stabilized zirconia (PSZ).

Partially Stabilized Zirconia

The term "partially stabilized zirconia (PSZ)" refers to a composition with insufficient stabilizer to retain 100 percent cubic upon cooling. Either a monoclinic or metastable tetragonal phase also forms. PSZ's have been fabricated by hot pressing zirconia powder to zirconia fabrics, each of which has a different stabilizer content (ref. 13) and by sintering a mechanical mixture of pure and fully stabilized powder (ref. 16). The most widely used method, however, is to react zirconia powder with an oxide or carbonate of the desired stabilizer.

The phase diagrams for the systems $CaO–ZrO_2$, $MgO–ZrO_2$, and $Y_2O_3–ZrO_2$ are shown in figures 6 to 8. The equilibrium diagrams predict at room temperature a two-phase mixture of monoclinic zirconia and another phase, the identity of which depends on the system (MgO for $MgO–ZrO_2$, $CaZr_4O_9$ for $CaO–ZrO_2$, and $Zr_3Y_4O_{12}$ for $Y_2O_3–ZrO_2$). This mixture is rarely obtained, however, because of the low rates of cation diffusion. It has been found that for compositions in the low-solute, tetragonal-cubic, solid-solution regions of the phase diagram (the shaded areas in figs. 6 to 8) suitable heat treatment can result in metastable retention of the tetragonal phase on cooling. A typical heat treatment (ref. 14) consists of a solution anneal at a high enough temperature to become single phase (cubic). The material is then rapidly cooled through the two-phase region and the tetragonal phase is nucleated. A subsequent anneal in the two-phase region allows controlled growth of tetragonal precipitates by diffusion.

It has been observed that the tetragonal phase will not transform to monoclinic if it is in the form of small precipitates constrained within a matrix. In PSZ's the matrix is high-solute, cubic ZrO_2. However, tetragonal zirconia has been successfully retained in a number of ceramic matrices (ref. 17). When the tetragonal precipitates become large enough, they transform spontaneously on cooling. The precise reason for the precipitate size dependence on the tetragonal retention is not yet clear. The various factors that have been proposed as controlling include

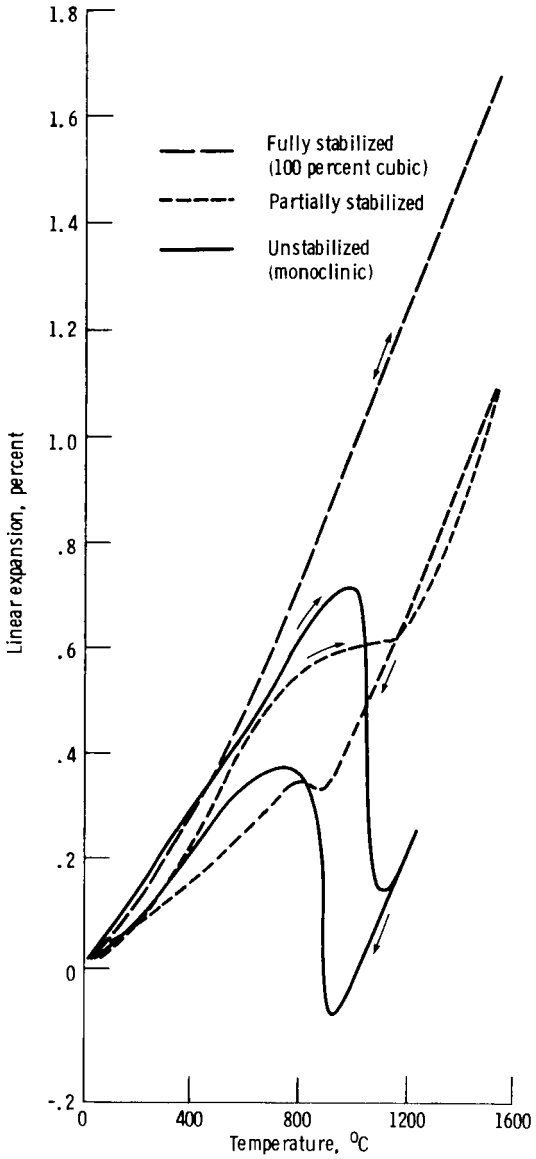

Figure 5. – Linear thermal expansion of unstabilized, partially stabilized, and fully stabilized zirconia. (From ref. 4.)

(1) Nucleation by dislocations – When the precipitates grow past a critical size, the interface strain becomes large enough to prevent the lattice planes, across the particle-matrix interface, from being continuous and dislocations must form. It has been suggested that these dislocations serve as nucleation sites for the transformation (refs. 18 and 19).

(2) Change in solute content – The composition of the precipitate should be a function of size. The chemical driving force for transformation is a function of composition. Possibly it is the change in composition, not the change in dimension, that is controlling (ref. 19). Studies of the precipitate chemistry are hampered by the small probe size (~1 nm) needed to obtain signals from only the precipitate.

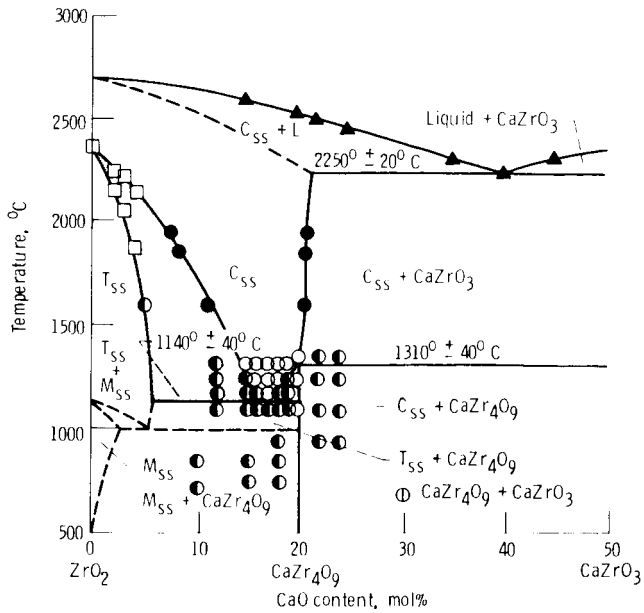

Figure 6. – Equilibrium phase diagram for system ZrO_2–CaO, where the subscript ss denotes solid solution. (From ref. 81.)

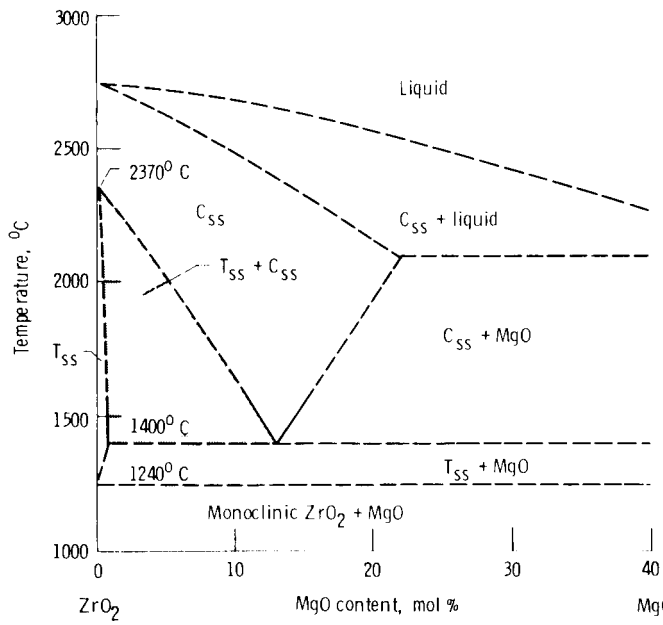

Figure 7. – Phase diagram for system ZrO_2–MgO. (From ref. 82.)

(3) Interfacial energy – Small particles, of course, have a higher surface-area-to-volume ratio than do larger ones. It has been suggested (ref. 20) that there is a penalty in surface energy (due to the loss of coherency) that must be balanced against the volume gain upon transformation (because monoclinic is the equilibrium form) and that a critical size must be obtained before this balance becomes favorable. This argument has been criticized because very small (5 nm) monoclinic particles, which by this reasoning should not have transformed, have been observed (ref. 26).

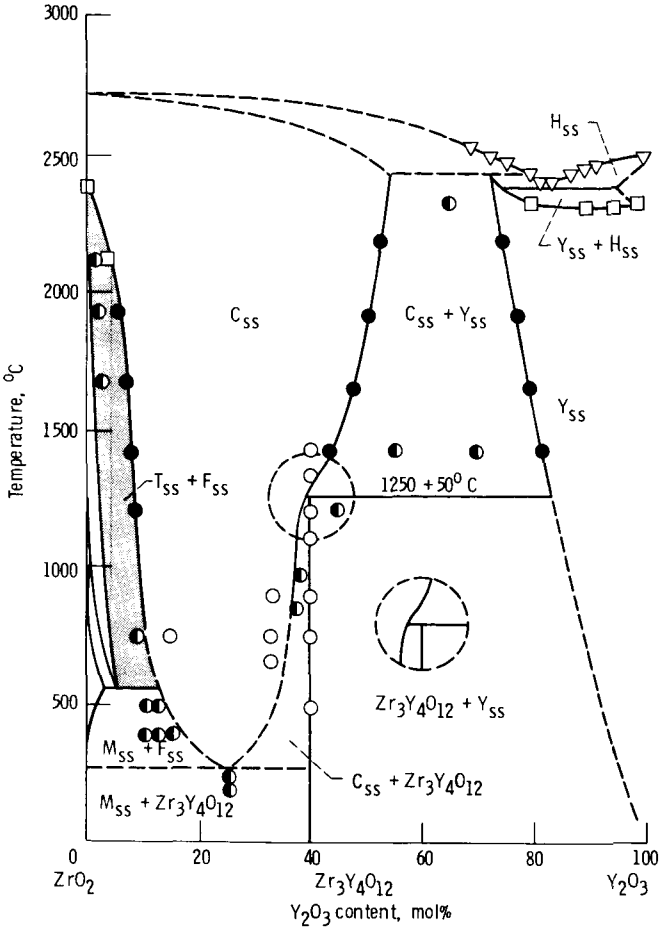

Figure 8. – Phase diagram for system ZrO_2-Y_2O_3. (From ref. 82.)

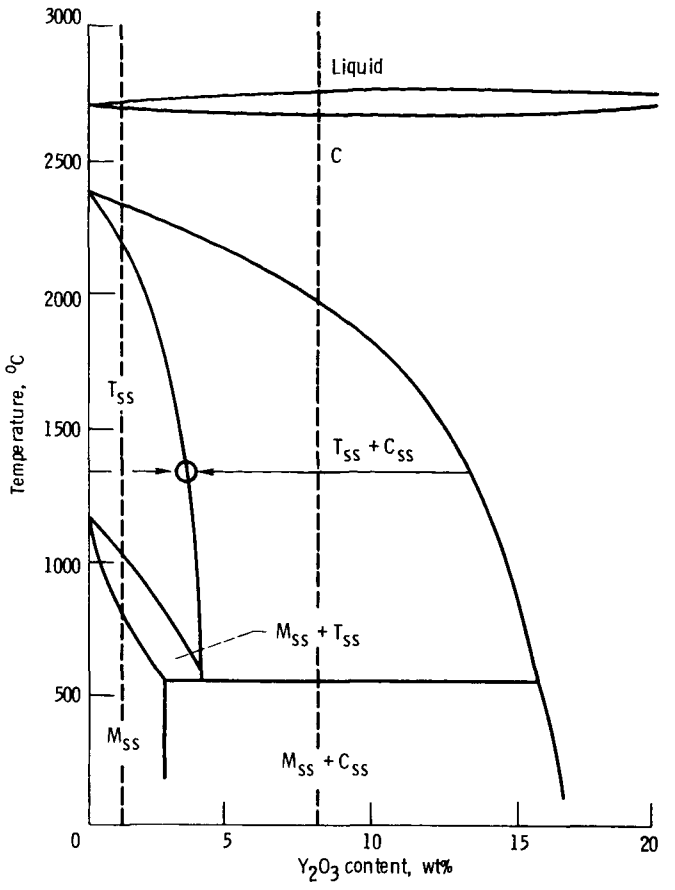

Figure 9. – Y_2O_3-ZrO_2 phase diagram indicating tetragonal phase whose transform behavior is sensitive to compositional direction of its origin. (From ref. 25.)

An additional phenomenon that occurs in Y-PSZ emphasizes the fact that retention of the tetragonal phase depends on precipitate-matrix interactions. The tetragonal phases when formed by decomposing a composition in the low-Y_2O_3 tetragonal field transform readily (refs. 15, 21, and 22); the same tetragonal phase when formed by decomposing a composition in a higher Y_2O_3 concentration (tetragonal plus cubic field) will not transform (refs. 21 and 22). This is schematically illustrated in figure 9.

Mechanical Properties—Room Temperature

The mechanical properties of partially stabilized zirconia depend on both the volume fraction and distribution of this tetragonal phase. The microstructure that results in the highest fracture toughness K_{Ic} and Young's modulus E for a dense ceramic is one in which there is a very high volume fraction (>50 percent) of very small precipitates ($\leq$10 nm). This is typically accomplished by the previously mentioned heat treatment. Materials prepared in this way are often referred to as "transformation toughened" (although this may be a misnomer for 8-mol % Y-PSZ). There are several excellent reviews on transformation toughening (refs. 19, 23, and 24). Only a summary is presented here.

Transformation toughening is accomplished by obtaining a microstructure that causes an energy-absorbing martensitic phase transformation to take place in the stress field ahead of an advancing crack tip. The first requirement for transformation toughening is that the precipitates be small enough to be metastably retained yet large enough to be transformed under stress. The second requirement is that the transformation be of a martensitic nature. A diffusional transformation could not provide accommodation on the small time scale needed. The characteristics of martensitic transformations are as follows (ref. 23):

(1) It involves a shape deformation, which as has been pointed out (ref. 25) is convenient experimental evidence of its occurrence. This transformation can be looked at as dissipating strain energy and thus demanding more work be done in order to propagate the crack.

(2) It is generally athermal. The amount of product formed is a function of temperature (or more precisely of undercooling) but not generally of time at temperature. This arises because the strains set up by the shape and

volume changes that occur cannot be relieved and the reaction is forced to cease before completion. When the temperature is further lowered, however, the increased driving force overcomes the opposing strain and the reaction proceeds. Note, however, that if the transformation takes place at a high enough temperature for the matrix strains to relax out (by, e.g., creep) the degree of completeness may depend on time. This may be the reason for the observation by Williamson (ref. 26) that at 950° C in pure ZrO_2 the transformation to monoclinic takes several weeks. It is also a possible explanation for the observation (ref. 27) that tetragonal precipitates in Mg-PSZ which are small enough to be metastably retained will transform upon annealing at 1000° C for 9 hr.

(3) It is a diffusionless reaction. No compositional rearrangements are necessary. The mol fraction of solute in the product (monoclinic) is the same as that in the parent phase (tetragonal). This is quite different from, for example, the phase reaction that takes place when a composition of 8-mol % Y-PSZ is cooled from 2500° to 1400° C. In this case, the products, approximately one-half cubic and one-half tetragonal, have concentrations of ~13-mol % Y_2O_3 and ~3 percent Y_2O_3, respectively.

The optimization mechanical properties of Mg-PSZ (ref. 14) and Ca-PSZ (ref. 28) are illustrated in figures 10 and 11, respectively. The initial point (time = 0) in both cases corresponds to material that has been solution annealed and quenched. The bend strength and fracture toughness increase with aging time up to a maximum. This is called peak-aged material. Note that the as-received[1] strength and toughness of Mg-PSZ are very near that of the peak-aged material, an indication that the production has been optimized well.

Two processes take place during aging. The first is the phase decomposition to the equilibrium mol fraction and the second, which is independent of the first, is the coarsening of the precipitates. When the material is quenched from the single-phase region, nucleation is a common event and the tetragonal phase initially consists of numerous small particles. To reduce the surface-area-to-volume ratio, as time proceeds the particles become less numerous and individually larger.

Several independent mechanisms can contribute to the observed toughening. The first, which was mentioned previously, arises from the transformation of the particles. When a crack propagates through a material, there is a stress field ahead of it. This induces the transformation to monoclinic with an unconstrained 4-percent volume increase. If the precipitates are homogeneously distributed, numerous, and small as compared with the crack dimensions, the material can be

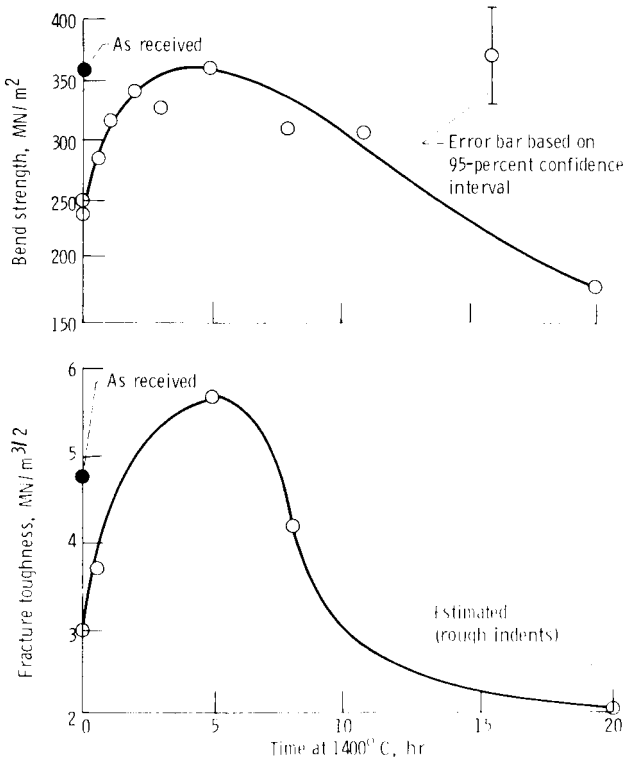

(a) Four-point bend strength.

(b) Fracture toughness (measured by overload microhardness indentations).

Figure 10. – Four-point bend strength and fracture toughness of solution-annealed 8.1-mol % Mg-PSZ as a function of aging time at 1400° C. (From ref. 14.)

treated as a continuum (ref. 30). The zone of transformed material would like to expand but is constrained from doing so. This results in a field of compression that the crack must overcome in order to propagate, as illustrated in figure 12.

When the precipitates are large enough and sparse enough to interact individually with the crack tip, the stress field applied by the precipitate will have a component that will tend to deflect the crack. Because such a deflected crack travels a more tortuous path than does a straight crack, more new surface area is produced per unit crack extension. This increased surface energy requires corresponding additional work for crack extension. In the absence of a transformation the crack may also be deflected by lattice, elastic, and thermal expansion mismatch between the matrix and the precipitate. This was demonstrated by fracturing 8-mol % Y-PSZ single crystals at temperatures above that of the transformation (ref. 31). That the fracture surfaces were rough implied a tortuous crack path forcing the same energy penalty as above.

Another possibility is that the energy released by the transformation is sufficient to cause microfracture of the

[1]The material was supplied by Zircoa Div., Corning Glass Works, Solon, Ohio.

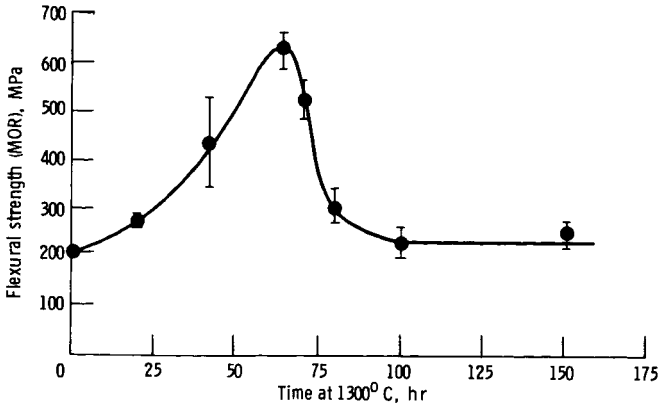

Figure 11. – Flexural strength of a 8.4-mol % CaO-PSZ alloy as a function of aging time at 1300° C. (From ref. 28.)

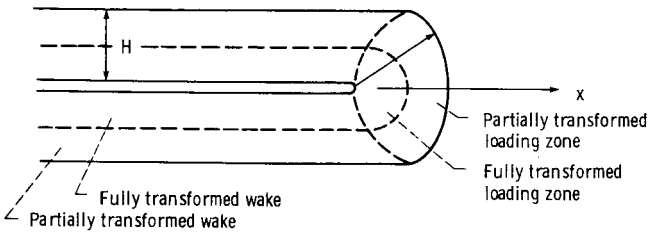

Figure 12. – Schematic of zone of transformed material during crack propagation. (From ref. 36.)

matrix. The microcracks thus produced create new surface and increase the compliance of the material. As long as they do not combine to form a critically sized flaw, their presence will contribute to toughening (ref. 32).

The contribution of microcracks to toughening in dense PSZ's is in question. Such microcracks have not been observed in PSZ's although they have been observed in other materials (e.g., zirconia-toughened Al_2O_3, ref. 17). In plasma-sprayed material that has a high density of microcracks, this may be a significant, perhaps the dominant, contribution overshadowing any contributions by the phase distribution.

Figures 10 and 11 show that aging past the peak is deleterious to the mechanical properties. This corresponds to the precipitates having grown past the critical size and having spontaneously transformed upon cooling. Their strain energy is spent (perhaps in the creation of a flaw) and is no longer available for crack inhibition. For Y-PSZ the situation is somewhat different. Work by Valentine (ref. 33) on 4.5-mol % Y-PSZ showed the fracture toughness to be essentially independent of aging (fig. 13) and low (~ 2.5 MN/m$^{3/2}$). However, work on low-yttria material (ref. 15)

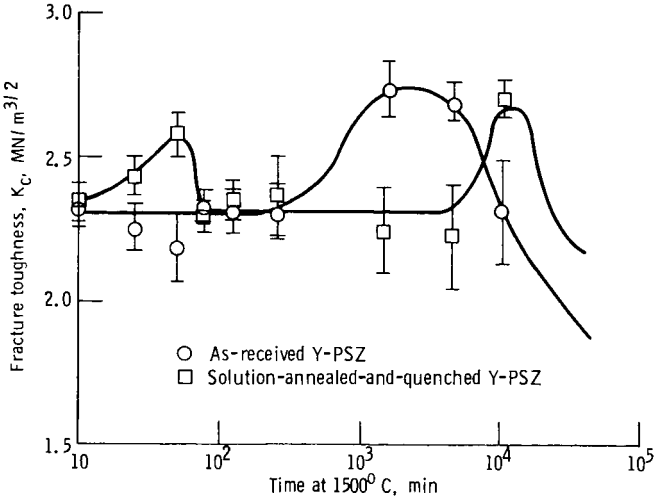

Figure 13. – Fracture toughnesses of as-received and solution-annealed-and-quenched 4.5-mol % Y-PSZ as a function of aging time at 1500° C. A Vickers diamond indenter and a 1-kg load were used for the fracture toughness measurements. (From ref. 33.)

(~ 1.4-mol % $YO_{1.5}$) has revealed high fracture toughnesses (6 to 9 MN/m$^{3/2}$) and high sensitivity to heat treatment. This sensitivity was correlated to grain size.

In summary, PSZ mechanisms are not completely understood. It is clear that the phase distribution of PSZ influences the mechanical properties. Also the phase distribution depends on the thermal history and can be controlled to give a strong, tough material.

Detection and Measurement of Phases in PSZ

The critical evidence for the phases present in a material is obtained by diffraction. Two common techniques are X-ray and electron diffraction. The latter has the advantage that it is done in an electron microscope and the investigator can examine and select the region from which the diffraction information will be obtained. Because the area examined by a typical X-ray diffractometer is much larger, the information is much more averaged and phases with small concentrations could be hidden.

There have been investigations of the phases in PSZ using both techniques on the same samples, and the results suggest that caution should be applied. Hannink, Johnston, Pascoe, and Garvie (ref. 28) investigated the phases present in Ca-PSZ as a function of aging at 1300° C. The surface was examined with X-rays after the anneal and then ground to transform the tetragonal and reexamined. For aging times less than 100 hr the monoclinic signal increased with grinding, as expected. For samples aged longer the monoclinic signal decreased with grinding. This was interpreted as showing that it is possible to transform monoclinic (in material with a high monoclinic fraction) back to tetragonal by applying stress. This is contrary to all other evidence, and it is far more likely that the CaO had evaporated from the near-

surface region and that the grinding had removed a layer of unstabilized zirconia. CaO has been observed to evaporate (ref. 34), as has MgO (ref. 14).

Mitsukashi, Ichihara, and Tatsuke (ref. 35) studied the phases in powders of zirconia. Very small (<10 nm) tetragonal particles gave X-ray patterns that appeared cubic. Larger tetragonal particles (~46 nm) would give cubic patterns if strained.

Hannink (ref. 18) studied the microstructures of Mg-PSZ, Ca-PSZ, and Y-PSZ. He found that for solution-annealed Ca-PSZ and Y-PSZ the X-ray patterns could be indexed only as tetragonal although transmission electron microscopy (TEM) showed the cubic phase to be present. He further found that, upon aging, the cubic X-ray pattern appeared and intensified (more clearly for the Ca-PSZ). The postulate offered was that the precipitates strained the lattice of the matrix (indicated by the X-ray peak width and the bright field TEM images) and that the matrix was more thoroughly strained by a large number of small precipitates (typical of solution annealing) than by a small number of larger precipitates (due to coarsening during aging).

Another complication arises from the existence of a second tetragonal phase in Y-PSZ. This is a phase formed by rapid quenching of the cubic phase and is distinct from the previously discussed low-solute, high-temperature, tetragonal phases (ref. 36). The lattice parameters of this phase are different from those of the ordinary tetragonal phase because it contains a different solute fraction. However, the differences are small and considerable overlapping of the peaks and spots occurs.

In light of this it is suggested that phase determinations should involve the use of TEM, at least to confirm the X-ray results. Also, materials such as the low-yttria material (believed to be 100 percent tetragonal, ref. 15), which have only been investigated by X-ray, warrant further examination by TEM. This material is worthy of further examination purely on the basis of its high fracture toughness.

Implications for Gas Turbine Applications

Gas turbine use of zirconia is currently restricted to coating-like forms and nonstructural applications. It is used on parts that are cyclically loaded by thermo-mechanical forces, where adhesion to the metallic substrate is the primary concern. Strength of the material is also important, particularly since failure often begins within the ceramic. The possibility of using monolithic components made of ceramic is currently under consideration, and in this case strength and toughness are critical.

The phase relationship and mechanical properties of zirconia have the following implications for gas turbine engine applications:

(1) The range of temperatures over which the material retains its structural integrity, and to what level, is an important consideration. Mg-PSZ and Ca-PSZ are optimized by anneals in the temperature range 1300° to 1400° C. However, long-term use at these temperatures is not possible because of the rapid kinetics of precipitate coarsening. Figures 10 and 11 show that with about 15 hr of additional aging after reaching the peak, all of the property enhancement is lost. This coupled with the problem of destabilization through solute evaporation, imposes a short use-time limit at high temperatures.

It has also been observed (ref. 14) that the structural integrity of Mg-PSZ is lost from annealing at 1000° C by a different mechanism. At this temperature the material undergoes a eutectoid decomposition; thus MgO is precipitated out at the grain boundaries and an increasingly less stabilized system is left. Only when annealing took place below 850° C did the microstructure remained unaltered.

A similar problem can be inferred for Ca-PSZ from the thermal shock data of Cooke and Popper (ref. 16) (although this was not their interpretation). They measured the retained strength after a water quench from high temperature. Figure 14 shows their results over the temperature range 920° to 1600° C. The divisions into regions A, B, and C are by the current author. Unfortunately, the time that the samples were held at temperature before quenching was not specified.

The observed behavior can be explained for the noted regions as follows: In region A the temperature was low enough so that the as-sintered microstructure was unaltered and gave the flat curve. In region B the system underwent eutectoid decomposition analogous to that described for Mg-PSZ, only with $CaZr_4O_3$ precipitated instead of the pure oxide. Such a reaction was predicted

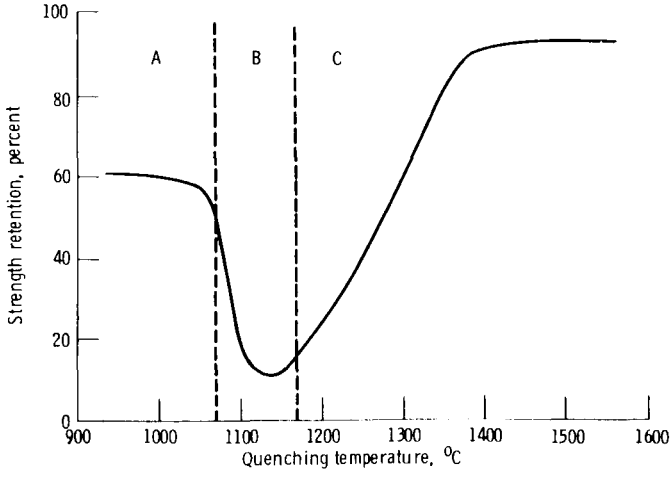

Figure 14. – Strength retention as a function of quenching temperature. (Letters A, B, and C denote division into regions by current author.) (From ref. 16.)

from the phase diagram (fig. 6). In region C the material developed a transformation-toughened microstructure by growth of the tetragonal phase. Although this is speculative, it is clear from Cooke and Popper's results that some reaction that produces unfavorable mechanical properties is taking place.

These findings point up the fact that under severe thermal conditions the prospect for the successful employment of Mg-PSZ or Ca-PSZ in the hot section of a gas turbine engine is doubtful. This correlates well with the finding of Stecura (ref. 37) that coatings of Ca-PSZ and Mg-PSZ failed much more rapidly than coatings of Y-PSZ when tested at 975° C.

(2) In Y-PSZ the phase changes are considerably more sluggish and the material is much more stable at high temperatures. The phase relations in plasma-sprayed material have been studied and found to be consistent with the expectations from the phase diagram (ref. 38). A correlation between the phase makeup and the lifetime has also been made (ref. 22). It remains, however, to show a cause and effect.

For plasma-sprayed Y-PSZ coatings the as-sprayed material contains a large fraction of the nonequilibrium tetragonal phase. The composition that contains the largest fraction of this phase also suffers the largest number of cycles to failure in a thermal shock test. This phase decomposes when aged at temperatures greater than 1200° C. It is important to determine if the properties that cause the coating to succeed truly depend on the presence of the nonequilibrium phase or not. It is also unlikely that transformation toughening makes any contribution in 8-mol % Y-PSZ since the observations are that the tetragonal (equilibrium) formed in this phase field does not transform.

(3) Since failure of these gas turbine systems often occurs in the ceramic, the possibility exists that a Y-PSZ that is transformation toughened will be advantageous. Obtaining such a structure would require a low-yttria composition and heat treating the material. The latter requirement is a difficulty because the temperature required is much higher than the metal substrate can withstand. It might be possible to age the material under a thermal gradient although the resultant microstructure would be optimized only at one point in the zirconia; the rest would be underaged or overaged.

A possible method for achieving a PSZ by plasma spraying is to use a mechanical mixture of fully stabilized and unstabilized powders. Although this would probably produce a nonuniform microstructure, mechanically mixed and sintered PSZ's (refs. 13 and 16) do display better strength and toughness than fully stabilized zirconia. It may make a great deal of difference whether the powder fully melts and whether the molten drops contain one or many particles, as well as the degree to which the drop homogenizes in flight. Therefore spray parameters would be very important.

Fabrication of separate zirconia components that would then be heat treated before attachment to the metal is another possibility that could have significant potential.

Thermal Conductivity

Basic Mechanisms for Dielectric Materials

The flux of heat through a material depends on the thermal gradient across the material and can be expressed as (ref. 39)

$$\frac{\partial Q}{\partial t} = -kA\frac{\partial T}{\partial x}$$

where

$\partial Q/\partial T$	flux of heat in x direction, W/s
k	thermal conductivity, W/m K
A	area normal to x, m^2
$\partial T/\partial x$	thermal gradient, K/m

In the absence of convection the thermal conductivity is the sum of contributions by three mechanisms:

(1) Conduction by electrons
(2) Conduction by phonons
(3) Radiation by photons

The relative importance of each term depends on three aspects of the carrier: the specific heat c_i, the carrier speed v_i, and the mean free path l_i.

$$k_{\text{eff}} = \frac{1}{3}\sum_i c_i v_i l_i$$

In the case of metals the conduction electrons, which are loosely bonded, can be approximated as a free-electron Fermi gas (ref. 40). In this model the electrons are analogous to the molecules in a gas. Heat is transmitted in the form of kinetic energy through electron-electron collisions. As the temperature is raised, the mean free path and hence the conductivity are reduced. In dielectric solids (e.g., zirconia) the number of free electrons is always small and this mechanism makes a minor contribution. Contrary to metals, however, this mechanism's contribution rises with increasing temperature up to a point (ref. 39) as the population of free electrons increases faster than the rate of reduction of the mean free path.

A major contributor in dielectrics is conduction by phonons. A phonon is a quantum of energy, analogous to a photon, from elastic waves propagating through the lattice. The temperature dependence of phonon conduction shows a maximum. At low temperatures the conduction increases with temperature because of the increase in specific heat predicted by Debye theory (ref. 39). Above a certain temperature the phonon-phonon interactions begin to reduce the mean free path, and conductivity drops. When the mean free path becomes as small as the lattice spacing, conductivity becomes independent of temperature.

The radiation contribution to thermal conductivity in solids is often small enough to be neglected although situations arise in which it is dominant. The radiation contribution always increases with increasing temperature and is a strong function of temperature.

Note that whenever the mean free path of any carrier becomes larger than the dimensions of the specimen, the effective mean free path is that dimension (ref. 39). This becomes important at low temperatures or small sizes.

Thermal Conductivity of Zirconia

The thermal conductivity of zirconia has been measured by many investigators. The data are characterized by a good deal of scatter (ref. 41). This scatter arises partially because the conductivity is small and therefore difficult to measure. Conductivity data for pure ZrO_2, Ca-stabilized zirconia, Mg-stabilized zirconia, and Y-stabilized zirconia are shown in figure 15. It seems that the thermal conductivity does not depend strongly on stabilization. The differences between the curves are within experimental scatter of each other and are not systematic.

Garvie has likened the conductivity of Ca-stabilized zirconia to that of glass (ref. 42). In this model the anion vacancies, which are produced by incorporating the stabilizer according to the reaction

$$CaO \xrightarrow{ZrO_2} Ca''_{Zr} + V_O^{\cdot\cdot} + O_O^X$$

act to scatter phonons. Garvie assumed a concentration of vacancies equal to 20 mol % and predicted a phonon mean free path of a body cell diagonal. The results agree very well with the values and temperature dependence results of one of the experimental studies referenced (ref. 43[2]); see figure 16. However, the other study referenced (which does not appear in his figure) has a temperature dependence of equal magnitude but opposite sign; see figure 17.

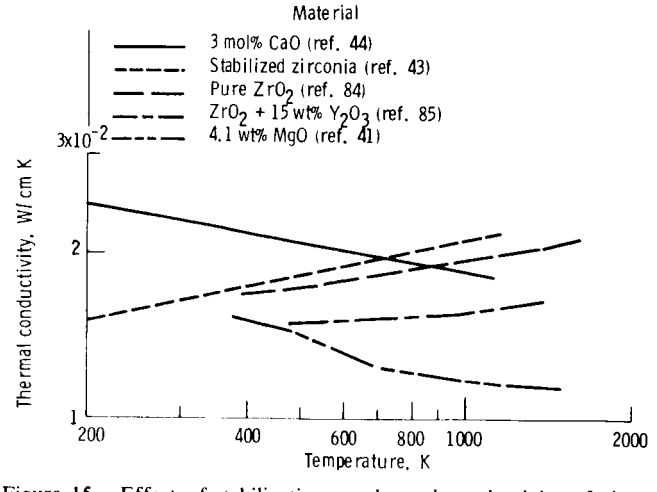

Figure 15. – Effect of stabilization on thermal conductivity of zirconia. (From ref. 41.)

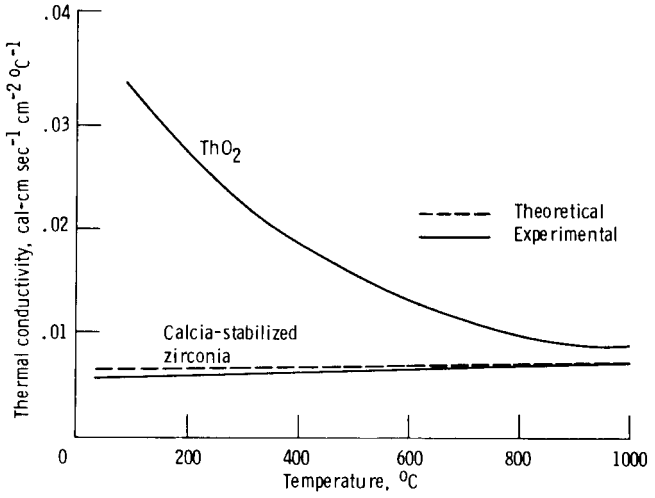

Figure 16. – Thermal conductivity of thoria and calcia-stabilized zirconia. (From ref. 45.)

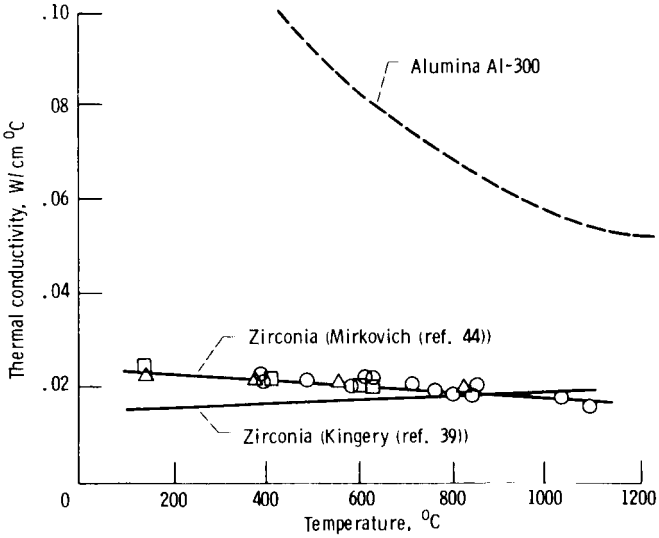

Figure 17. – Thermal conductivity of zirconia, using Pyroceram 9606 and alumina (Al-300) standards.

[2]Note in both ref. 42 (Garvie) and ref. 45 (Mirkovich) the incorrect reference is given for what should be ref. 43, Kingery, et al.

There are other problems with Garvie's model. If the phonon mean free path is governed by the presence of anion vacancies, which in turn are fixed by the stabilizer concentration, a large difference in thermal conductivity between pure and stabilized zirconia is predicted. This was not observed (fig. 15).

The data of Mirkovich (ref. 44) came from a sample containing only 3.35-mol % CaO (Kingery et al.'s data (ref. 43) are unspecified), and yet they are of very nearly the same magnitude as those calculated by Garvie. Even if the material had fully phase separated into a matrix of fully cubic zirconia with a high stabilizer content and low-stabilizer-content precipitates, the matrix would constitute less than 10 percent of the volume. For the matrix to dominate in this case would require it to have a conductivity much higher than pure ZrO_2. Not only was this not observed, but it is contrary to the prediction of this model.

Measurements of the thermal conductivity and specific heat of fully yttria-stabilized zirconia at very low temperatures (0.1 to 20 K) have also shown that zirconia has "glassy characteristics" (ref. 45). It was found that at these low temperatures the phonon mean free path was limited by the presence of highly localized excitations, which have been used to explain the thermal conductivity behavior in a number of glassy materials. The origin of these excitations is not known. A lack of data on unstabilized zirconia prevents a determination of whether the disorder from which they arise is intrinsic or produced during stabilization. Note that at these low temperatures the measured mean free paths are of the order of 40 μm, which is much greater than the distance separating the anion vacancies in 8-mol % Y-stabilized zirconia. Measurements of this type on well-characterized single crystals would be very desirable in order to find the source of these excitations.

The radiation contribution to thermal conduction in zirconia has been largely neglected except for a study of plasma-sprayed material (ref. 46). This contribution is very dependent on the microstructure (scattering centers in the form of pores, inclusions, or precipitates limit photon mean free path), the surface condition (emittance depends on roughness and spectral absorption of the surrounding medium), and the sample dimensions.

Thermal Conductivity of Plasma-Sprayed Zirconia

The thermal conductivity of plasma-sprayed Y-PSZ has been reported in two thermal (stress-heat transfer) studies. Liebert and Stepka (ref. 47) give the thermal conductivity for $400 \leq T \leq 1900$ K as

$$k(\text{W/m K}) = -1.597 + 0.011\ \text{T} - 1.896 \times 10^{-5}\ T^2 + 1.324 \times 10^{-8}\ T^3 - 3.077 \times 10^{-12}\ T^4$$

Taylor (ref. 48) gives data points that can be satisfactorily fit by

$$k(\text{W/m K}) = 0.651 - 8.465 \times 10^{-4}\ T + 1.719 \times 10^{-6}\ T^2 - 1.420 \times 10^{-9}\ T^3 + 4.678 \times 10^{-13}\ T^4$$

Plots of these functions are shown in figure 18. The Liebert and Stepka curve shows structure that has no explanation and probably resulted from fitting too few data points with too high an order polynomial. Structure aside, both curves indicate a strong temperature dependence, $\sim T^{1.5}$. This is in contrast to the very weak temperature dependence for conventionally processed ZrO_2 (fig. 17) and indicates that the conductivity is governed by a different mechanism.

Plasma spraying produces a porous material that contains microcracks. In a material with interconnected porosity and interparticle cracks, both radiation and gas-phase conduction can be expected to play a role. In the work of Wilkes and Lagedrost (ref. 49) as well as that of Bogonov, Pirogov, and Makarov (ref. 50), the thermal conductivity of plasma-sprayed zirconia was found to be very dependent on the type and pressure of the atmosphere present. That the conductivity increased with increasing pressure indicates that gas conduction is indeed a contributor.

These workers' measurements in a vacuum also show large temperature dependences (figs. 19 and 20); the first heatup cycle of Wilkes and Lagedrost is shown in these figures; the others are discussed later. This temperature dependency is not as high as the T^3 typically given for radiation. However, the T^3 dependence holds only for gray bodies, which zirconia is not.

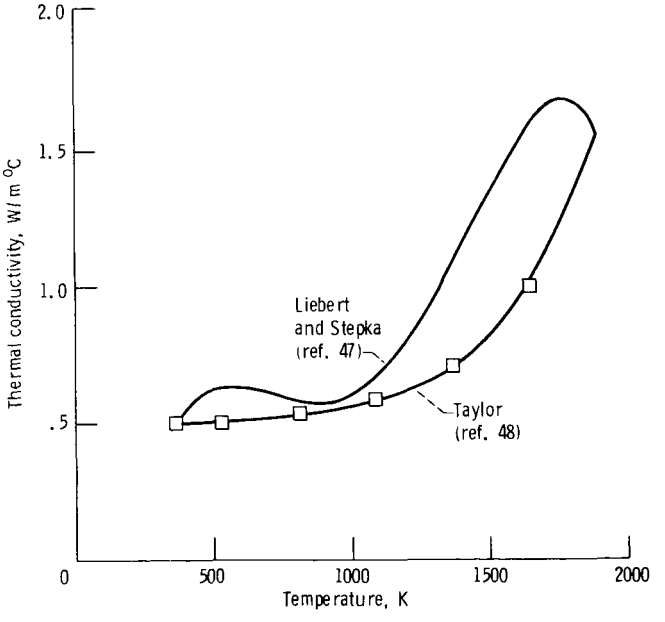

Figure 18. – Thermal conductivity of plasma-sprayed zirconia.

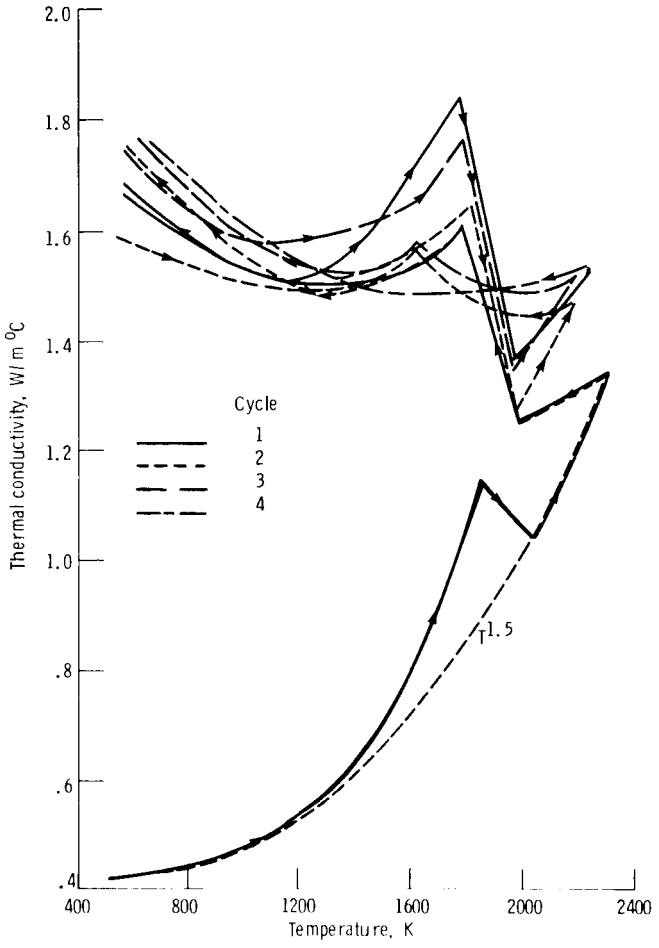

Figure 19. – Thermal conductivity of plasma-sprayed Ca-PSZ in a vacuum. (From ref. 49.)

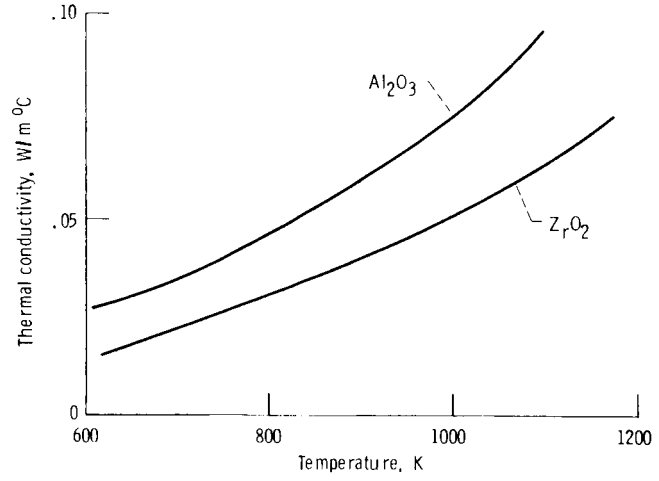

Figure 20. – Thermal conductivity of plasma-sprayed alumina and stabilized (unspecified) zirconia in a vacuum. (From ref. 50.)

Kingery et al. (ref. 39) point out that the photon mean free path is a function of wavelength in dielectric solids and increases with decreasing wavelength. It is suggested that this should increase the temperature dependence since the peak emission for a blackbody shifts to shorter

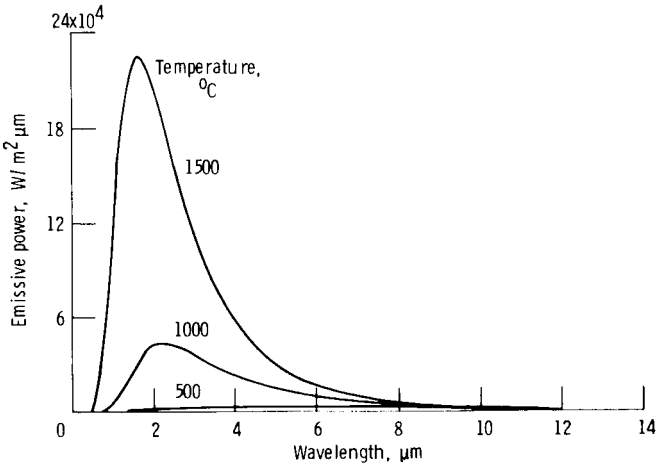

Figure 21. – Spectral emissive power of a blackbody as a function of temperature.

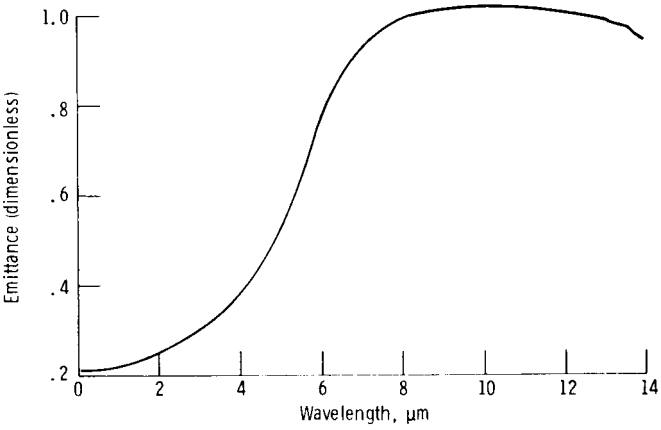

Figure 22. – Spectral emittance of plasma-sprayed zirconia. (Data from ref. 46.)

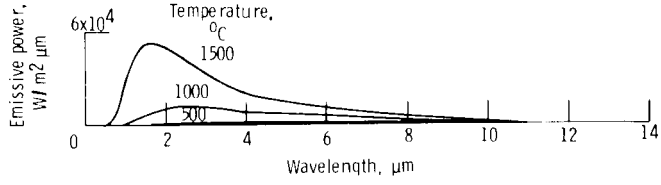

Figure 23. – Spectral emissive power of zirconia.

wavelengths at higher temperatures (fig. 22). However, the fact that the emittance of zirconia is very low, approximately 0.2 to 0.25 in this short-wavelength region (fig. 22), must be taken into account. The emission from zirconia is the convolution of the curve in figure 21 with that in figure 22 and is shown in figure 23. This curve is far less biased toward the short wavelengths than a blackbody and this will tend to diminish the temperature dependence.

To make a quantitative estimate of the radiation using

$$k_r = \frac{1}{3}\int C_r(\lambda)\, v_r(\lambda)\, l_r(\lambda)\, d\lambda$$

all of the variables must be known as a function of wavelength, which they are not. The work of Boganov et al. (ref. 50) is indirect evidence to support radiation dominance.

It was observed that the conductivities of the coatings prepared from stabilized ZrO_2 and Al_2O_3 are very nearly the same (fig. 20), but the conductivities of dense Al_2O_3 and ZrO_2 in this temperature range are quite different (fig. 17). If radiation were dominant, the similar spectral emittances of Al_2O_3 and ZrO_2 (ref. 41) would result in similar conductivities.

Another aspect of the work of Wilkes and Lagedrost (ref. 49) is the effect of thermal history on the conductivity. They found that after heating through the first cycle, the conductivity lost its temperature dependence and remained between 1.7 and 1.5 W/m^2 K. (The peak at ~1800 K was attributed to the evaporation of CaO, and it did not appear in the Y-PSZ.) They did observe sintering with diatometer measurements as have others (an example, from the work of Gaffin (ref. 51), is shown in fig. 24). Pretest and post-test metallography was also performed by Lagedrost and Wilkes. The results, shown in figure 25, reveal a significant difference. The pretest microstructure is characterized by small cracks between the individual particles. These cracks allow very small contact area between the particles for conduction but are good locations for radiation. In the post-test microstructure (that which underwent a heat treatment) the interparticle cracks have sintered and left a row of fine voids, which will presumably coalesce. The result is a more continuous matrix and the conductivity will increasingly reflect conduction.

The lack of quantitative sintering data and radiation estimates makes it difficult to separate the contributions to the thermal conductivity and the effect of heat treatment on them.

Implications for Gas Turbine Applications

The thermal conductivity of zirconia has the following implications for gas turbine engine applications:

(1) The dramatic change in thermal conductivity with thermal cycling calls into question the practice of judging

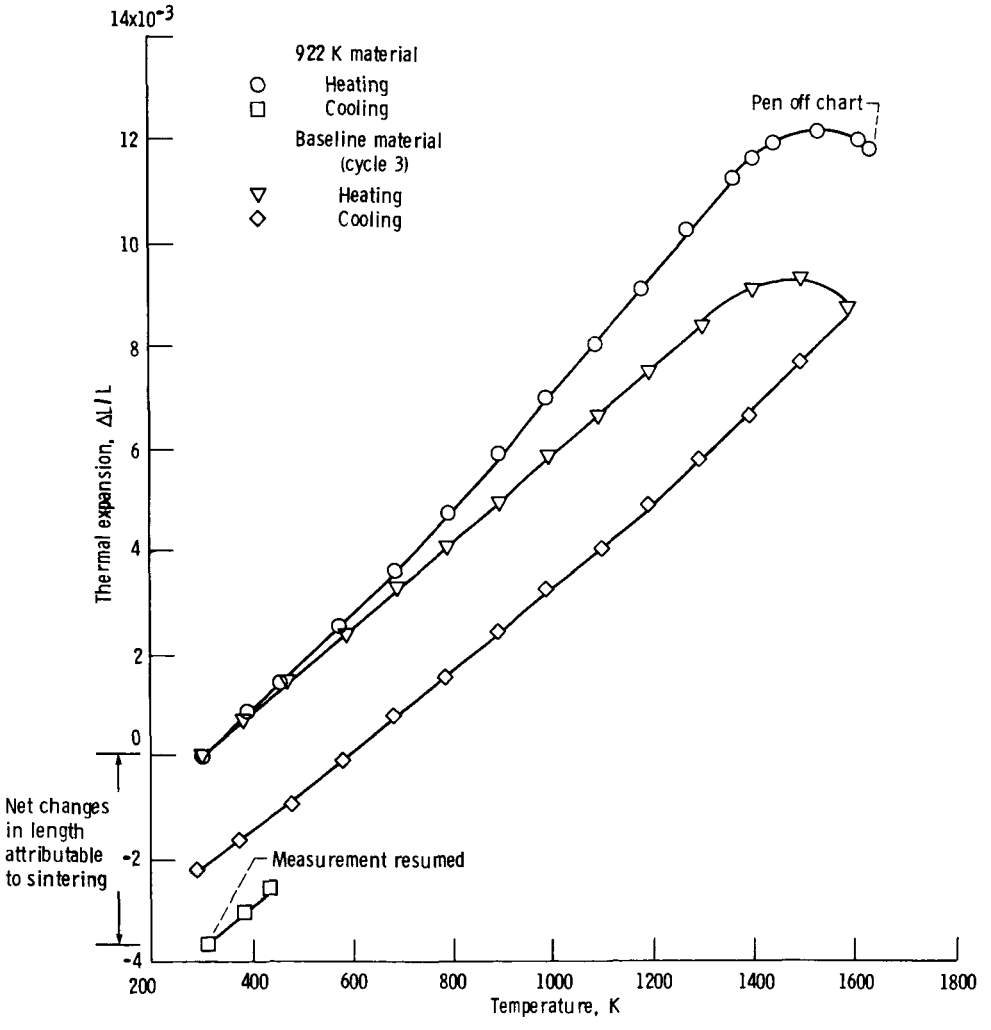

Figure 24. – Thermal expansivity of plasma-sprayed zirconia (first cycle). (From ref. 51.)

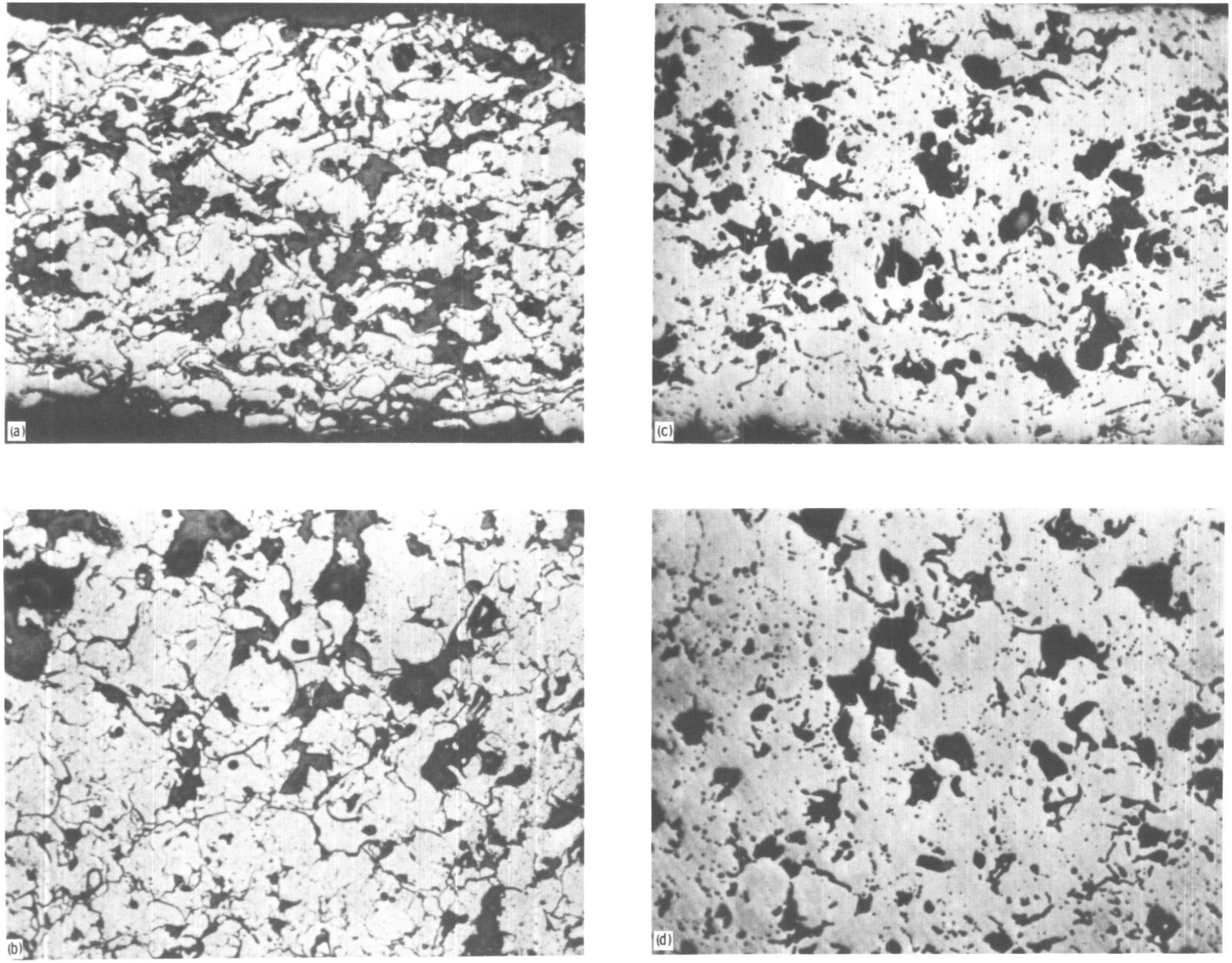

(a) As sprayed, longitudinal section.
(b) As sprayed, transverse section.
(c) After measurement, longitudinal section.
(d) After measurement, transverse section.

Figure 25. – Metallography of plasma-sprayed CaO–PSZ. (From ref. 49. All specimens as polished.)

the behavior of a plasma-sprayed zirconia from measurements made in the as-sprayed state. The use of as-sprayed thermal conductivity in heat transfer and thermal stress calculations results in values that are appropriate only for very short use times.

(2) The thermal conductivity of dense material is very low, and the observation that plasma-sprayed material rapidly becomes as conductive as dense material suggests that no insulation penalty will be incurred by the use of dense material.

(3) There remain questions about the mechanisms of thermal conductivity in both plasma-sprayed and dense ZrO_2.

Deformation

The deformation of materials can be divided into two categories: elastic and plastic. Elastic deformation is common in ceramic materials at low temperatures. In this case the strain is related to the applied stress simply by the moduli:

$$\sigma = E\epsilon$$

where

σ normal stress
E Young's modulus
ϵ normal strain

and

$$\tau = G\gamma$$

where

τ shear stress
G shear modulus
γ shear strain

When the stress is removed, all of the elastic strain is recovered. At high temperatures ($T/T_m > 0.5$, where T_m is the melting temperature) the materials can undergo permanent strain, or plastic deformation. There are a number of mechanisms by which this can occur. Reviews of the high-temperature deformation behavior are available, including those by Terwilliger and Radford (ref. 52) and Kingery, Bowen, and Uhlmann (ref. 39).

Deformation by Slip

One very important method by which deformation can occur is "slip." Slip is the movement of planes of atoms, one over another. In a perfect crystal slip occurs when the entire lattice plane cooperatively shifts by the shortest repeat distance (i.e., until the atoms are in sites equivalent to their initial sites). Although the energy of such an action is prohibitively high, the presence of dislocations allows small regions of material to slip successively.

Figure 26(a) illustrates an edge dislocation (in which the slip direction is perpendicular to the dislocation line) and figure 26(b), a screw dislocation (in which the slip direction is parallel to the dislocation line). A dislocation is a line defect that separates the region of slipped material from the unslipped. Dislocations are often thought of as an extra half-plane of atoms. This can be seen in the illustration of slip by edge dislocation motion (fig. 27). The energy for slip then can be thought of as the energy for dislocation motion. Anisotropy of the crystal structure can cause the energy to be a function of orientation. In metals, where local space charges do not occur, close-packed directions are favored because of the short repeat distance. In ionic solids, however, electrostatic repulsion can interfere, and slip along directions favorable by packing may not occur.

Specific crystals have specific slip systems. A slip system is written as $\{hkl\}\ \langle uvw \rangle$, where hkl are the crystallographic indices of the slip plane and uvw those of the slip direction. The applied stress to cause slip is that which yields a resolved shear stress greater than the critical resolved shear stress given by (ref. 39)

$$\tau = \frac{F}{A} \cos\varphi \cos\psi$$

where

τ resolved shear stress

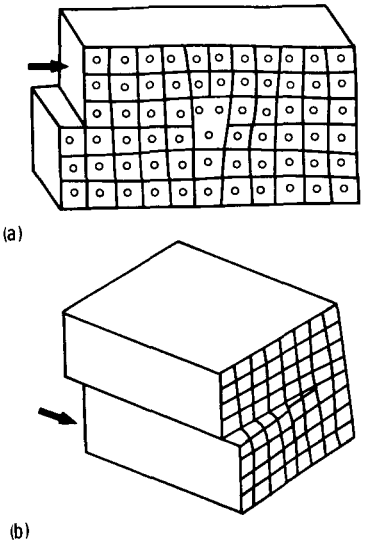

(a) Pure edge dislocations.
(b) Pure screw dislocations.

Figure 26. – Pure edge and screw dislocations occurring during plastic deformation. (From ref. 39.)

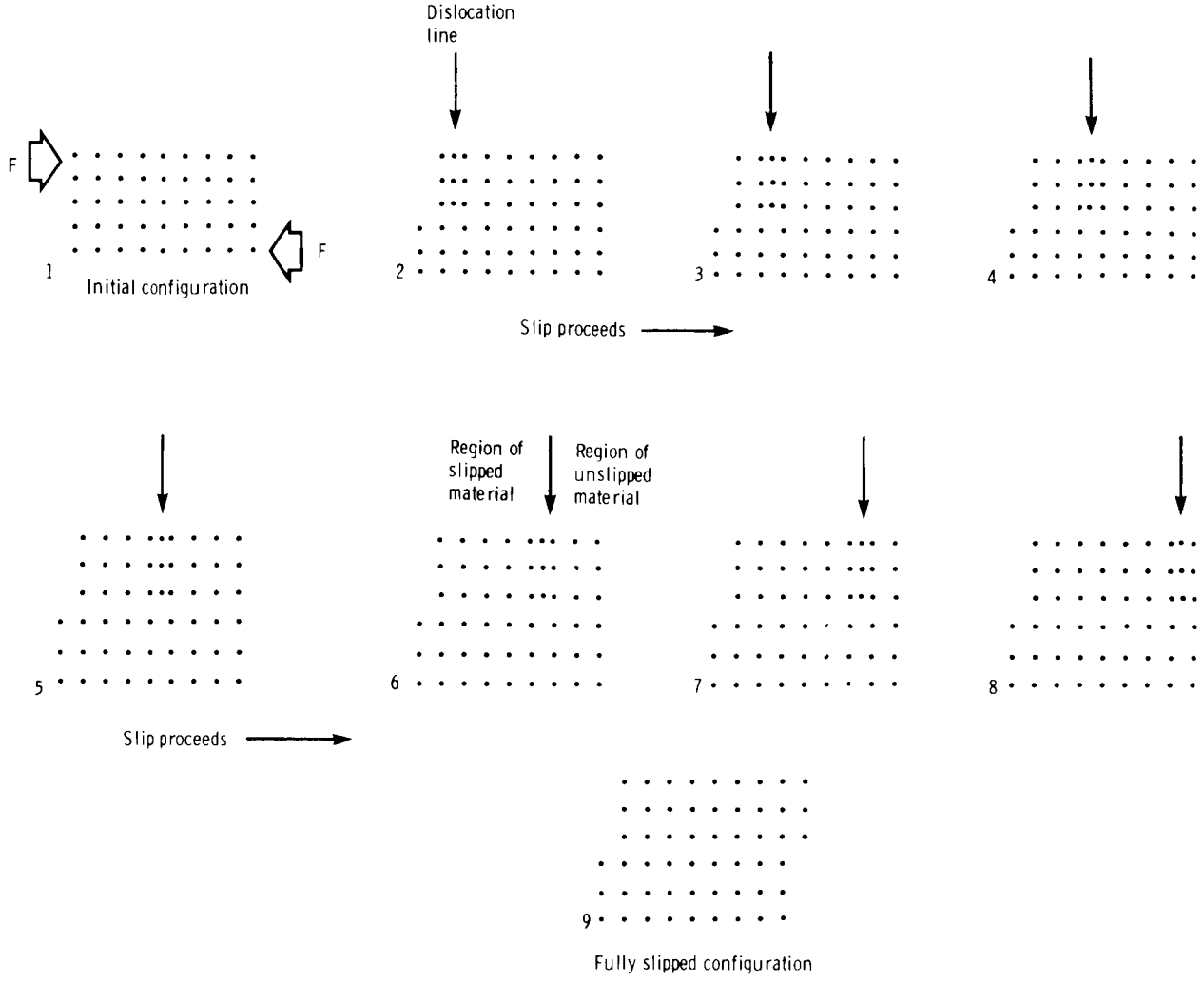

Figure 27. – Illustration of dislocation motion during deformation by slip.

F applied force

A cross-sectional area of sample

φ angle between slip plane and loading axis

ψ angle between slip direction and loading axis

The term $\cos \varphi \cos \psi$ is called the Schmid factor. The situation is illustrated in figure 28. As the temperature is increased, less applied stress is necessary simply because the background of thermal energy is higher. This may allow slip systems with higher thresholds, termed secondary slip systems, to operate.

Materials with the fluorite structure (e.g., fully stabilized zirconia and the matrix in PSZ) typically have three low-temperature slip systems, {100} ⟨110⟩. At high temperatures there are two additional systems, {111} ⟨110⟩ and {100} ⟨110⟩. Experimental determination of the slip systems in Ca-stabilized zirconia agrees with the above (ref. 11). At high levels of deformation the dislocation population may become dense enough that motion is impeded by dislocation-dislocation interactions; this gives rise to strain hardening. Several additional aspects need to be considered for polycrystalline materials. Obstacles to dislocation motion arise in the form of second phases and grain boundaries. Because inclusions, precipitates, and pores prevent the dislocation from proceeding along its original path, it must expend additional energy to climb (by diffusion) around the obstacle or it may remain pinned and cease to contribute to the deformation. Grain boundaries are often regions into which impurities segregate and thus create a barrier. The crystallographic misalignment from one grain to another, even with atomically clean boundaries, can block shear. Von Mises (ref. 53) and Taylor (ref. 54) have determined that five independent slip systems are necessary for ductility in polycrystalline ceramics.

At high temperatures zirconia, will satisfy the requirement for five independent slip systems. Al_2O_3, however, has only two low-temperature slip systems (ref. 39), the basal systems {0001} ⟨1120⟩. At high temperatures slip can occur on both the prismatic and pyramidal

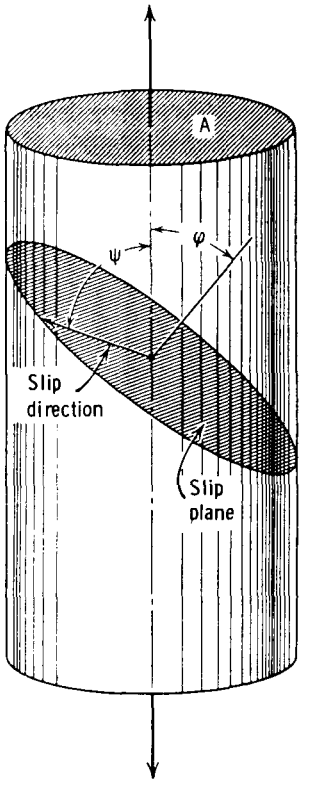

Figure 28. – Determination of critical shear stress. (From ref. 39).

systems; however, the stress to initiate slip in these systems is 10 times that of the basal, even at 1700° C. As a consequence the deformation of Al_2O_3 is very anisotropic. On this basis it is apparent that it is inappropriate to relate the plastic deformation of polycrystalline PSZ to that of polycrystalline Al_2O_3 on the basis of the homologous temperature T/T_m as has been suggested (ref. 55).

Diffusion-Controlled Deformation

Another method by which mass transport can occur is through the motion of atoms, or diffusion. Diffusion is a thermally activated process and therefore makes more significant contributions at high temperatures. The dislocation climb mentioned in the previous section requires diffusion. It is also possible for recovery, the removal of dislocation entanglements, to take place by diffusion. Strain can also be produced directly from a diffusive flow to relieve the applied stress gradient.

The diffusion coefficient of an atomic species is directly related to the diffusion coefficient of the defect species responsible for transport by

$$D_a = f c_d D_d$$

where

D_a diffusion coefficient of atomic species

D_d diffusion coefficient of defect

c_d defect concentration

f correlation coefficient

From this it can be seen that the atom mobility can be increased by increasing the concentration of defects. This may be effected by doping (added low-level impurities) or by changing the atmosphere (e.g., altering the partial pressure of oxygen).

However, increasing the defect concentration may not lead straightforwardly to an increase in the ease of deformation. For example, doping Al_2O_3 with Ti^{+4} is believed to increase the number of oxygen interstitials (ref. 56) by the reaction

$$2Al_i + 3TiO_2 \xrightarrow{Al_2O_3} 3Ti_{Al} + \frac{3}{2}O_i'' + 6O_O^x + Al_{Al}^x$$

These interstitials are bound to the titanium in a cluster, and rather than contributing to mass transport the clusters serve as traps for dislocations. The material is strengthened rather than weakened (ref. 57).

In zirconia the effect of increasing the stabilizer concentration is to increase the concentration of oxygen vacancies. For example,

$$CaO \xrightarrow{ZrO_2} Ca_{Zr}'' + V_O^{\cdot\cdot} + O_O^x$$

The creep rate of this material goes through a maximum. It increases for stabilizer additions up to ~15-mol % CaO and then decreases with further additions (ref. 58); see figure 29. The ionic conductivity, which is controlled by the concentration and mobility of oxygen vacancies, also goes through a maximum at the same point (ref. 59); see figure 30. The increase in both properties up to ~15-mol % CaO can be ascribed to the increasing stabilization (i.e., the decreasing content of tetragonal and monoclinic phases).

The decrease in the single-phase cubic material with increasing stabilizer can be explained by defect interaction. At these high concentrations the vacancies see each other's strain field and space charge. It has been proposed that a superlattice of ordered vacancies forms. Evidence for this is in the form of diffuse electron scattering (ref. 60), electrical conductivity losses (ref. 61), and an increase in microhardness (ref. 62). The degree of ordering will depend on the driving force (an inverse function of temperature) and the kinetics (a direct function of temperature). The referenced results suggest that ordering is maximized at 1000° C.

Diffusive creep should be limited by the slowest-moving species. It is shown in the next section that this is the cations rather than the oxygen. As Porter (ref. 62)

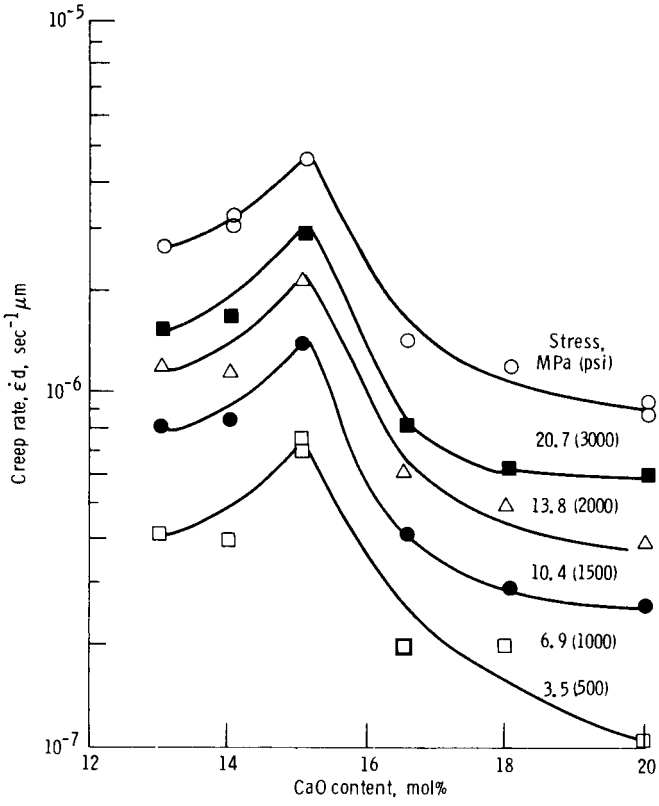

Figure 29. – Log-normalized creep rate as a function of CaO content at 1350° C for various stresses. (From ref. 58.)

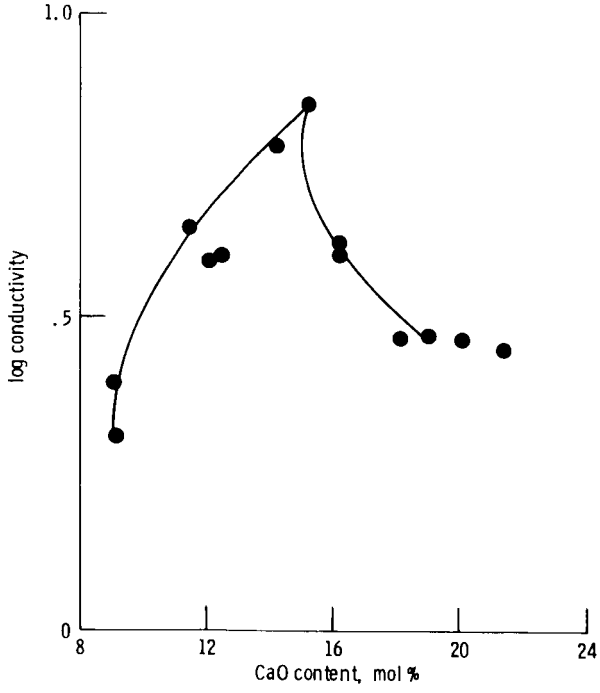

Figure 30. – Ionic conductivity as a function of CaO content at 1400° C. (From ref. 59.)

points out, however, the ordering of anion vacancies can alter the magnitude of the shortest repeat distance (called the Burger's vector of the dislocation), and the presence of ordered domains will act as a barrier to dislocation motion. Porter also points out that this is analogous to the effect of ordering, γ phase $\rightarrow \gamma'$ (ordered) phase, observed in superalloys.

Zirconia is a material that can tolerate significant nonstoichiometry. The concentration of oxygen vacancies increases as the oxygen partial pressure is reduced by the reactions

$$O_O^x \rightarrow \frac{1}{2}Og(g) + V_O^{\cdot\cdot} + 2e^-$$

Terwilliger and Radford (ref. 52) point out that many off-stoichiometry materials show increased deformation because of greater disorder. Zirconia might be expected not to show increased deformation on the basis of the ordering argument. In addition, it is also noted that TiO_2 (which has four slip systems, $\{101\}\langle 101\rangle$, $\{110\}\langle 001\rangle$) is stronger when it is off-stoichiometry because of the interaction of dislocations with the vacancies. In cubic zirconia, which also has high symmetry, it is possible that the trapping of dislocations outweighs any enhanced diffusion. The creep rate is reduced by a factor of 10 when 10-mol % Y-PSZ is deformed in a vacuum (fig. 31).

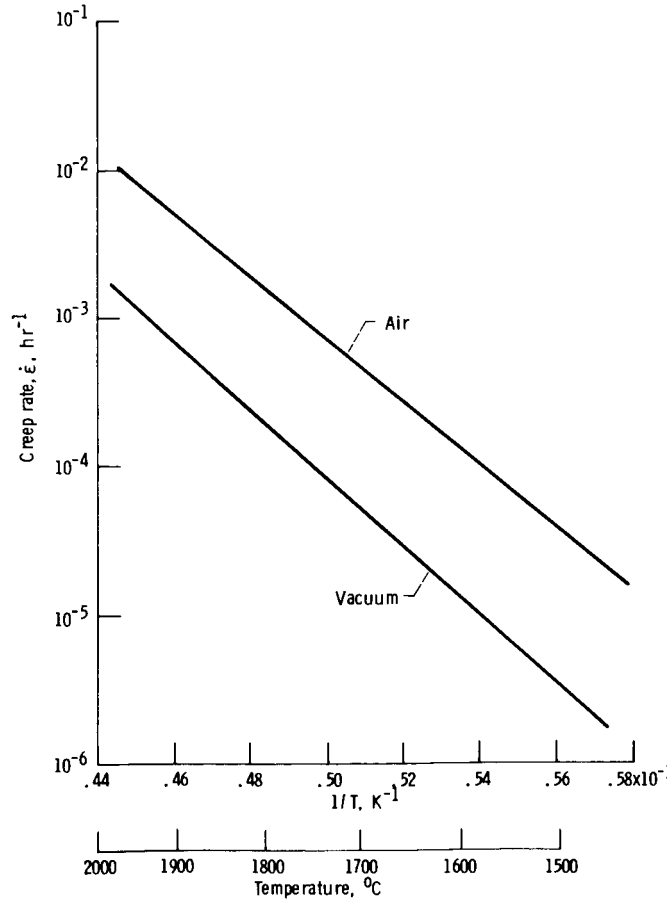

Figure 31. – Steady-state creep rate as a function of reciprocal absolute temperature for high-density YSZ tested in compression.

Deformation by Grain Boundary Sliding

In polycrystals the sliding of grains across each other can contribute to deformation. In dense material the sliding of interior grains is constrained by neighbors and stresses build up. These stresses must be relieved through the dislocation motion or diffusion (ref. 63), which may be controlling factors. In porous materials the accommodation requirements are much less severe and the deformation becomes more dependent on the nature of the boundaries (e.g., impurity segregation and interfacial contact area); see figures 32 and 33.

Experimental data for the effect of porosity on the creep rate of Al_2O_3 are shown in figure 34. A very large effect can be seen. In very impure materials it is possible to have a glassy ($SiO_2 + \Sigma X_i$) phase at the grain boundary. This may allow viscous flow to assist the deformation and may provide a fast path for diffusion. During grain boundary sliding it is possible to nucleate cavities (stress-driven pores) that may coalesce and lead to failure.

The effect of the presence of grain boundaries on the mechanical properties of zirconia is clearly seen in the work of Ingel, Lewis, Bender, and Rice (ref. 31). Their measurements of the flexural strength of polycrystalline Mg-PSZ and a single crystal of Y-PSZ versus temperature are shown in figure 35. The strength of the polycrystalline material is much lower at all temperatures

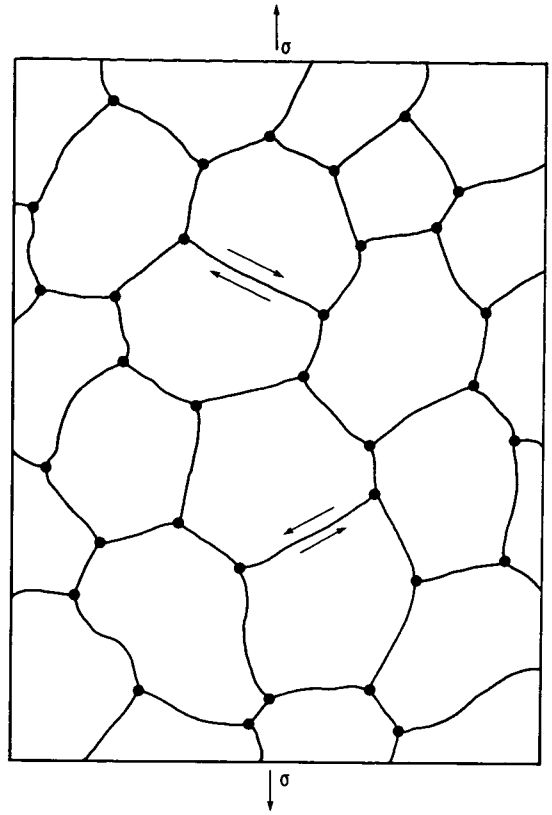

Figure 33. – Sliding in a porous compact. (Requirements for accommodation are considerably relaxed by internal pore surfaces.) (From ref. 63.)

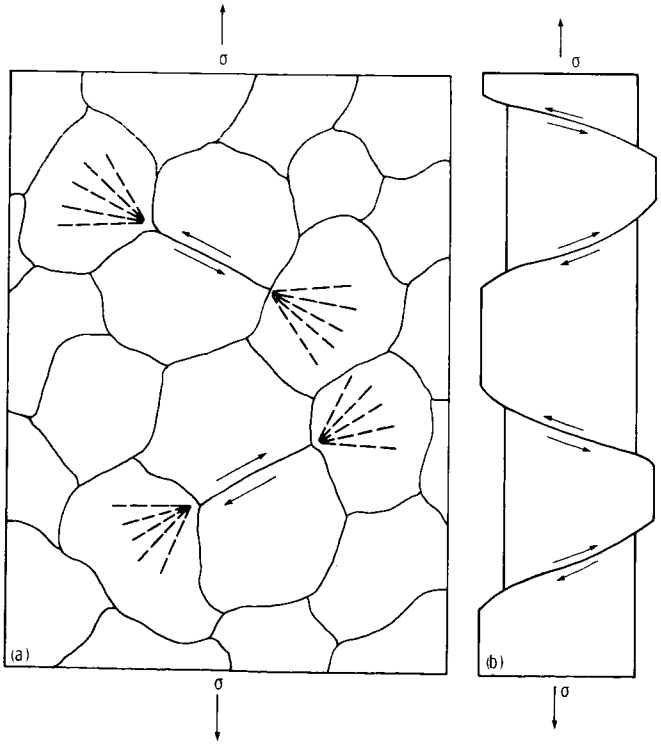

(a) Constrained grain boundary.
(b) Free grain boundary sliding (ref. 84).

Figure 32. – Accommodated grain boundary sliding, where σ is applied stress. (From ref. 63.)

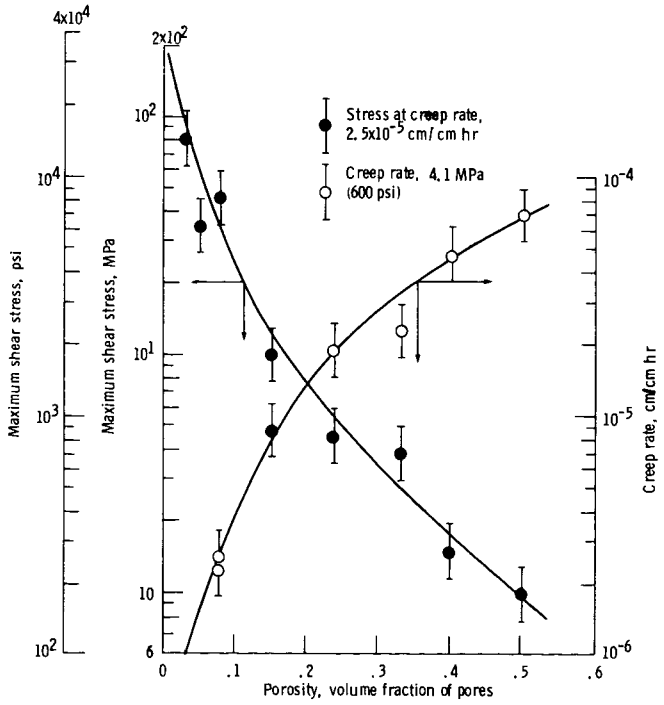

Figure 34. – Creep of polycrystalline alumina as a function of porosity. (From ref. 39.)

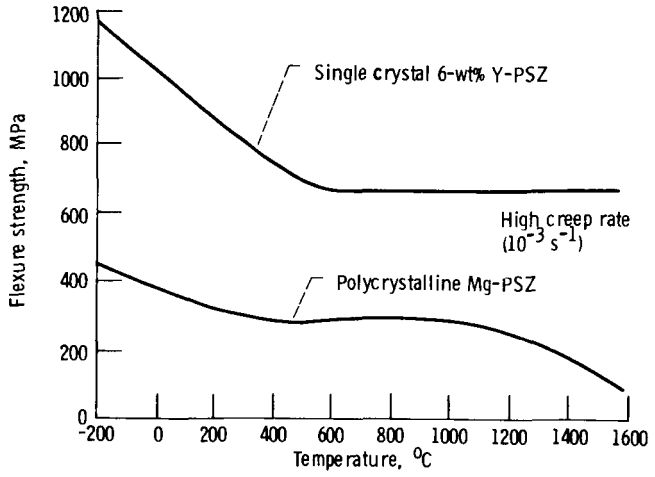

Figure 35. – Flexural strength of partially and fully stabilized zirconia single crystals, polycrystalline PSZ, and hot-pressed Si_3N_4 (HPSN) as a function of temperature. (From ref. 31.)

and drops off to an almost negligible amount at temperatures greater than 1400° C. An even more striking contrast shows up in their measurements of fracture toughness (fig. 36), in which the single-crystal toughness increases markedly at high temperatures while the polycrystalline toughness drops steadily with temperature.

Deformation of Plasma-Sprayed Zirconia

Plasma spraying, as previously mentioned, produces a porous material with residual stress. The effect of porosity, reduction of the accommodation requirement, is amplified by the fact that the pores (interparticle cracks included) are very acicular. This, as mentioned in the section Thermal Conductivity, results in a small contact area between particles. A distinction is made between grains and plasma-sprayed particles that may be polycrystalline.

Creep studies indicate, as might be expected, that plasma-sprayed zirconia deforms primarily by particle sliding (ref. 64). All of these tests were done in compression. Because of the brittle nature of most ceramics, tensile testing is rarely employed since grip alignment is critical. Compressive loading is favored, although the interpretation of the results can be difficult. When a cylinder of material is compressed along its axis, it attempts to expand radially. However, in a compressive test the ends of the cylinder are constrained by friction. This produces a radial compressive stress on the sample with a maximum at the ends and dropping off toward the center. The sample is not under unaxial compression but rather under a biaxial gradient. The interpretation of the load-deflection curve is no longer straightforward and it is difficult to be quantitative. Precisely this difficulty occurred in reference 16 and the primary mode of deformation was "barreling." Barreling is meant to describe a radial expansion in the sample center (fig. 37).

A meaningful creep test for plasma-sprayed material is needed.

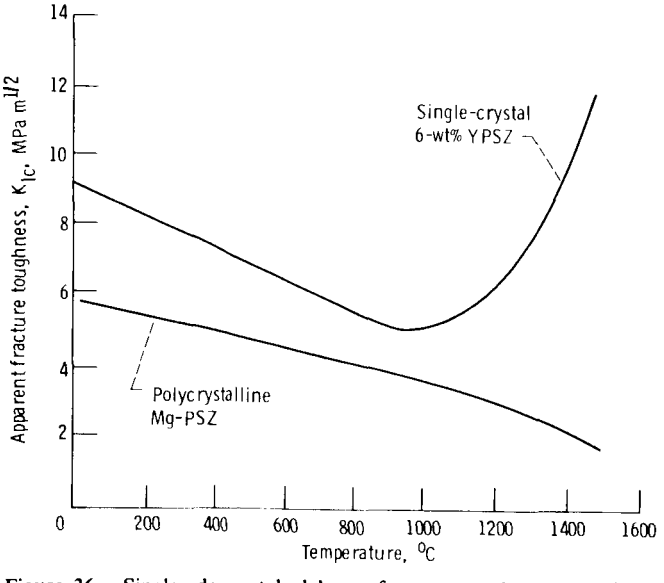

Figure 36. – Single-edge notched beam fracture toughness as a function of temperature for single-crystal Y-PSZ and polycrystalline PSZ. (From ref. 31.)

Implications for Gas Turbine Applications

The deformation behavior of zirconia has the following implications for gas turbine engine applications:

(1) It seems clearly, though qualitatively, indicated that the interparticle boundaries control the deformation behavior of plasma-sprayed zirconia. Sintering, as discussed in the section Thermal Conductivity, would be expected to have a large effect on the deformation. The acicular nature of the pores means that during sintering there is a large gain in interparticle area per unit

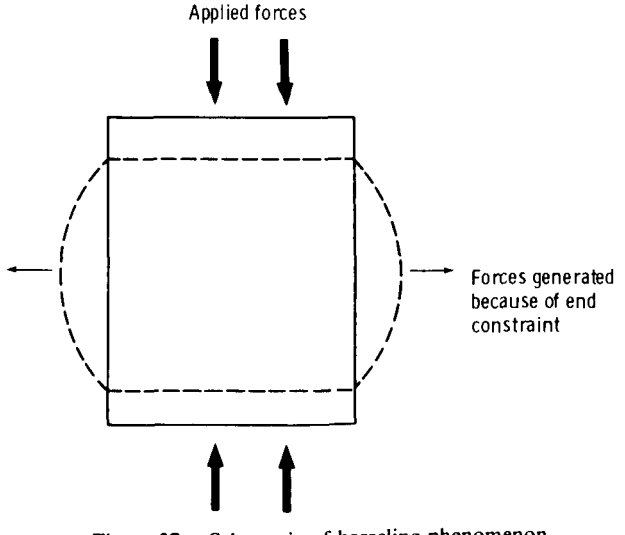

Figure 37. – Schematic of barreling phenomenon.

dimensional change. An effect of annealing on deformation was observed (ref. 55), though the authors attribute it to a different cause, in deadweight ball indentation tests at 1205° C. It was found that the ball penetrated twice as deeply into as-sprayed material as into material that had received a 24-hr anneal at 1278° C. The microstructures were not investigated.

This reinforces concern over the choice of input data for programs designed to predict stress and strain. In addition, the time-at-temperature dependence of creep rate complicates the determination of the stress-free temperature. Sometimes substrates are prestressed to give compression on the ceramic. It is an open question whether the fast creep rate during the first heating cycle is rapid enough to cause this prestress to be lost.

(2) For a material in which the grain boundaries control the deformation, as might be expected in plasma-sprayed materials, it is an advantage to have clean boundaries. It has been observed (ref. 65) that adding Al_2O_3 (which does not react with ZrO_2 below 1600° C and only forms a solid solution above 1600° C) to sintered ZrO_2 produces a more ionically conductive material. Examination of the material by TEM revealed that the discrete regions of Al_2O_3 acted as sinks for the impurities (primarily SiO_2), which are normally distributed along the grain boundaries. The cleaner boundaries translate into the increased conductivity. Although it has not been tested, such material would be expected to show less deformation at high temperatures because of the absence of a glassy grain boundary phase. Using such material for gas turbine applications would require high-temperature anneals for the necessary diffusion to occur. This would involve the same problems mentioned in the section Phase Relationships and Mechanical Properties.

Diffusion

The rate at which matter can be transported through a material is important for a number of processes. The deformation behavior, as just discussed, may depend on diffusion. Ionic conductivity depends on the mobility of the ions. Other processes that involve mass transport are sintering or phase decomposition, and the value of a material as a barrier depends on the rate of transport across it.

In a system in which diffusion is in one direction x, the flux density is described by Fick's first law

$$J_i = -D_i \frac{\partial c_i}{\partial x}$$

where

J_i flux density of i^{th} species, mol/m^2-sec
D_i diffusion coefficient of i^{th} species, m^2/sec
c_i concentration of i^{th} species, mol/m^3
x position, m

Diffusion in Dense Zirconia

Stabilized zirconia, as pointed out by Rhodes and Carter (ref. 66), is an unusual material in that the diffusion taking place on the anion sublattice is much faster than that on the cation sublattice. They found that, in 12-mol % Ca-PSZ, the diffusion could be described by

$$D_{Ca} = 0.444 \exp\left[\frac{-100.2 \text{ (kcal/mol K)}}{RT}\right], \text{ cm}^2/\text{sec}$$

$$D_{Zr} = 0.035 \exp\left[\frac{-92.5 \text{ (kcal/mol K)}}{RT}\right], \text{ cm}^2/\text{sec}$$

Oxygen diffusion in 14.2-mol % Ca-PSZ was described by Simpson and Carter (ref. 67) as

$$D_O = 0.018 \exp\left[\frac{-31.2 \text{ (kcal/mol K)}}{RT}\right], \text{ cm}^2/\text{sec}$$

The permeation of oxygen through 8-mol % Ca-PSZ was studied by Smith, Meszaros, and Amata (ref. 68). Because of a discrepancy between their results and early work of Kingery et al. (ref. 69), they proposed that holes were controlling the rate of permeation. However, from the agreement between their work and the tracer measurements of Simpson and Carter the control seems more likely to be oxygen vacancies. The permeation results can be described by

$$D_O = 185 \exp\left[\frac{-57.6 \text{ (kcal/mol K)}}{RT}\right], \text{ cm}^2/\text{sec}$$

All of these results are shown in the Arrhenius plot in figure 38. The quite good agreement between the permeation and tracer studies is evident. It is also clear that the anion diffusion is by far the more rapid, $D_O/D_{Ca} \sim 10^6$, and that the activation energy for anion diffusion (the slope of the curve is a measure of the activation energy) is much lower than that for cation diffusion.

Carter and Roth (ref. 59) found that the activation energy for ionic conduction (which is proportional to diffusion) increased at a constant temperature with increasing stabilizer concentration. This is consistent with the hypothesis of anion ordering. At high stabilizer concentrations the activation energy contains an addition term, the heat of the order-disorder transition.

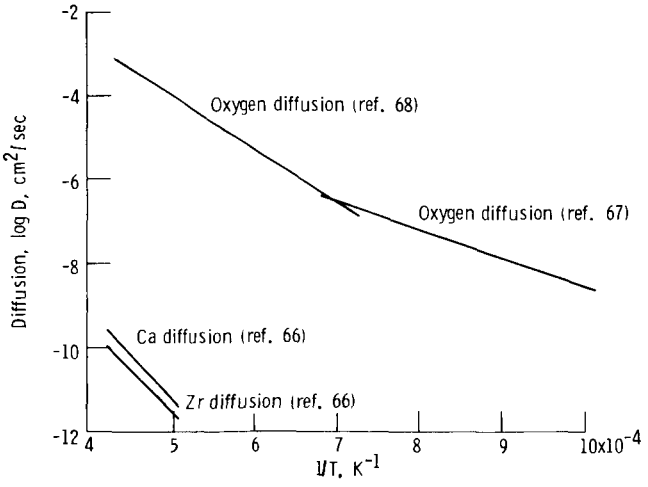

Figure 38. – Arrhenius plot of anion and cation diffusion in Ca-PSZ.

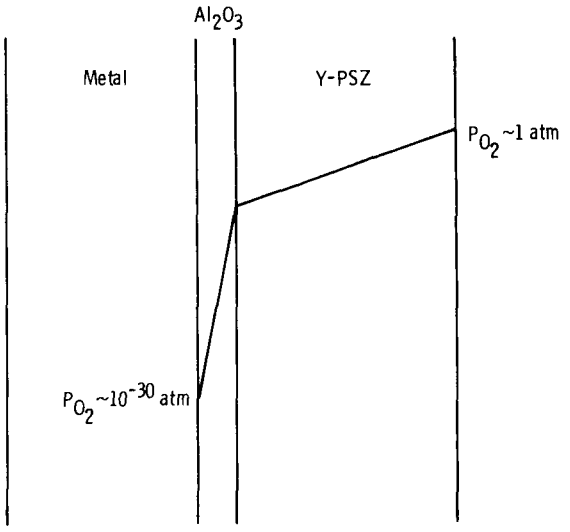

Figure 39. – Schematic of gradient in oxygen partial pressure across zirconia metal system in gas turbines.

The fact that oxygen diffusion is extrinsic is confirmed by its independence of oxygen partial pressure (ref. 69). The amount of defects produced by reducing the material is small with respect to those produced by stabilizing.

The implication is that processes controlled by mass transport in PSZ will be controlled by cation diffusion. On the basis of precipitation kinetics, $D_{Mg} > D_{Ca} > D_Y$. Measurements of interdiffusion in the fluorite-cubic solid solutions suggest that the diffusion of Mg is slightly greater than that of Ca (ref. 70).

Diffusion in Porous Materials

In porous materials, under an activity gradient, the situation becomes considerably more complex. The extra factors that now need to be addressed include

(1) The diffusion coefficient for the gas phase, generally much greater than that in the solid

(2) The volume fraction pore phase and the size-shape distribution. A distribution of discrete pores with mean diameter of the order of a gas molecule diameter would give markedly different behavior than a series of columnar pores that extend from one surface to the other, even if they both represent the same volume fraction. In addition, in the class of columnar pores the tortuosity of the path can vary greatly and affect the rate of diffusion.

(3) Convective flow. The presence, or absence, of convective flow can have a large effect on mass transport. This effect also depends on the size distribution of the pore phase.

(4) Stability of pore distribution. To predict the material's behavior, it is necessary to know the stability of the pore distribution over time. For example, the character of the system can change from columnar to discrete pores during use at high temperature.

Diffusion in Plasma-Sprayed Zirconia

Plasma-sprayed zirconia is indeed a porous structure (~10-vol % pores) although its porosity depends on the spray parameters. In gas turbine applications there is an activity gradient across the material (fig. 39). The diffusion coefficient of O_2 in air at 0° C is 0.178 cm²/sec (ref. 71). From the change in the viscosity of air the diffusion coefficient at 1200° C is estimated to be ~0.058 cm²/sec. This is ~10^4 greater than the oxygen diffusion in the solid. Clearly, the gas phase in the porosity may be the dominant contributor.

As mentioned, the pore distribution must be known and stable for quantitative assessment of the gas-phase diffusion. It is neither. Figure 25 shows that the pore distribution changes rapidly. In the as-sprayed condition the porosity is much more interconnected. This is evidenced by the fact that precursors (e.g., polyester), which are sometimes used, may be burned out by low-temperature (~500° C) anneals (ref. 51). Quantitative and systematic study of the pore phase morphology, including microcracks, is needed.

Implications for Gas Turbine Applications

The diffusion of zirconia has the following implications for gas turbine applications:

(1) Since the crystallographic stability of the PSZ is governed by cation diffusion, the formation of defect complexes with the stabilizer that are less mobile than free ions could increase longevity. One method of possibly obtaining these complexes is to use more than one stabilizer.

(2) One of the considerations that prompted the use of plasma-sprayed ceramics was the oxidation of the metal parts. A major factor in the oxidation rate is the temperature, which is substantially reduced when the ceramic is in place. It would be an additional advantage to have the PSZ also serve as a barrier to oxygen although as a barrier its use is restricted by the high value of D_O. Using PSZ as a barrier requires dense material and no cracking. This might be obtained by a heat treatment in an inert atmosphere after spraying or by a new fabrication method. Along this line the work of Bill, Sovey, and Allen (ref. 72) showed that the number of thermal cycles to failure was increased by incorporating 2 μm of radiofrequency-sputtered dense Y-PSZ between the metal and the plasma-sprayed Y-PSZ. A metallographic examination was not done, and it is speculative to ascribe this gain to a reduction in bond coat oxidation. However, it would be consistent with the observation.

Chemical Reactivity of Zirconia

The chemical reactions that take place between the constituents of a system become increasingly important as the temperature increases and can determine the lifetime of the system.

For any particular material there are an infinite number of chemical reactions to be considered simply because an infinite number of reaction couples can be constructed. It is necessary to be restrictive to be meaningful. The following discussion will be focused on zirconia in relation to engine component materials (such as the NiCrAlY or CoCrAlY alloys) or to materials under consideration and combustion products from the fuel. Although it is common to seek a system that is as inert as possible, all chemical reactions are not deleterious. An example of a potentially beneficial reaction is the grain boundary scavenging reaction mentioned in the section Deformation. Clearly, any gross reaction that consumes or destabilizes the majority of the zirconia is undesirable. In addition, small-scale reactions that produce a liquid or gaseous product can be harmful.

Zaplatynsky (ref. 73) conducted a systematic investigation of the reaction of various carbonates and sulfates with 8-mol % Y-PSZ. The results can be broken down into four categories;

(1) Chemical compounds that did not react with the 8-mol % Y-PSZ: Na_2SO_4, K_2SO_4, Cr_2O_3, Al_2O_3, and NiO

(2) Chemical compounds that reacted to produce a new compound: Na_2CO_3, K_2CO_3, $BaSO_4$, and $SiO_2(NH_4)_2HPO_4$

(3) Chemical compounds that stabilized the PSZ, as evidenced by an increase in the ratio of cubic to monoclinic X-ray intensity: MgO, Fe_2O_3, $CoCO_3$, and ZnO

(4) Chemical compounds that destabilized the PSZ: $V_2O_5(NH_4)_2PO_4$ ($(NH_4)_2PO_4$ decomposes to P_2O_5 upon heating and P_2O_5 has been shown to destabilize both Ca-PSZ and Y-PSZ (ref. 74)). Those compounds that form new compounds and those that destabilize the material have obvious disadvantages. The stabilizers might also cause concern, however. In the case of Fe_2O_3 Japanese work (ref. 75) has indicated that the reaction was far more substantial than Zaplatynsky indicates. Of particular interest, it was reported that iron oxides react to a much greater extent with Y-PSZ than with either Mg-PSZ or Ca-PSZ. In general, the stabilization of zirconia will produce a volume change, the result of which is stress when the material is constrained. It would be desirable to have all of the stabilization take place before the attachment to the metal.

On the basis of Zaplatynsky's results the presence of Na_2SO_4 and K_2SO_4 would be not a cause for concern and the elimination of cobalt from the system is indicated. The work of Hodge, Miller, and Gedwill (ref. 76), however, shows the reverse to be true. They found that the sulfates of Na and K penetrated the ceramic and condensed and thus produced mechanical stresses that caused failure. Increasing the concentration of Cr or Al in the NiCrAlY or switching to CoCrAlY extended the lifetime. Also since CoCrAlY is known to have better sulfidation resistance than NiCrAlY, the probability of reaction decreases, which is consistent with their results, although they suggest that this is a secondary effect.

The failure by a corrosion-sulfidation mechanism of the bond coat was also put forth by Siemers and McKee (ref. 77). In addition they found, consistent with Zaplatynsky, that vanadium destabilized the material.

The reactions between Si_3N_4, as well as SiC, and ZrO_2 are also of interest since they are candidate materials for gas turbines. The investigations to date have taken place due to interest in either providing these materials with transformation toughening or using them as hot pressing aids. The result has been (ref. 78) that extensive reaction occurs. The implication is that a barrier would be needed between Si_3N_4 or SiC and ZrO_2 at high temperatures.

The chemical reactivity of zirconia has the following implications for gas turbine applications:

(1) Although the zirconia does not appear to be undergoing significant reaction with them, the sulfates are limiting the lifetime of the material by impregnation. An impermeable zirconia layer would allow greater freedom in choosing the composition to meet other requirements. Obtaining an impermeable layer might be tried as outlined in the section Diffusion.

(2) The tendency of Y-PSZ to react with iron oxides suggests that costabilization might be worth investigating, for example, $CaO + Y_2O_3 + ZrO_2$.

Summary of Results

This literature review on zirconia with respect to gas turbine applications suggested the following points:

1. Cation diffusion in Ca-PSZ (partially stabilized zirconia) and Mg-PSZ is sufficiently rapid that these materials are unsuitable for advanced gas turbine applications.

2. The microstructure of the plasma-sprayed Y-PSZ has a great bearing on the properties of interest, and the effect of aging at use-temperatures has also been recognized to alter these properties in a significant way. However, a systematic study of the evolution of the microstructure is still lacking, especially with plasma-sprayed materials.

3. There are indications that monolithic, dense components, which may be isothermally heat treated, could show improved behavior

a. In developing a microstructure that will lead to increased toughness

b. Such monolithic components might have higher temperature capabilities than superalloys in current use or other ceramics such as SiC and Si_3N_4.

4. Very thin, dense films of ZrO_2 might serve as a barrier against oxidation and corrosion of the underlying metal.

5. There remain many unknowns about zirconia: for example, why the thermal conductivity of zirconia is so low and so independent of impurities and why the same tetragonal phase in Y-PSZ is transformable when arrived at from a low-yttria composition and not transformable when approached from a high-yttria composition.

6. The existence of an ordered oxygen vacancy superlattice is still not conclusively proven.

Studies leading to the answers to these types of questions will further the fundamental knowledge needed to make accurate predictions of the material's behavior.

National Aeronautics and Space Administration
Lewis Research Center
Cleveland, Ohio, November 10, 1983

References

1. Anthony, A. M.: High Temperature Refractory Applications of Zirconia. The Science and Technology of Zirconia, A. H. Heuer and L. W. Hobbs, eds., American Ceramic Society, 1981, pp. 437-454.
2. Issacs, H. S.: Zirconia Fuel Cells and Electrolyzers. The Science and Technology of Zirconia, A. H. Heuer and L. W. Hobbs, eds., American Ceramic Society, 1981, pp. 406-418.
3. Subbarao, E. C.: Zirconia - An Overview. The Science and Technology of Zirconia, A. H. Heuer and L. W. Hobbs, eds., American Ceramic Society, 1981, pp. 1-24.
4. Butze, H. F. and Liebert, C. H.: Effect or Ceramic Coating of JT8D Combustor Liner on Maximum Liner Temperatures and Other Combustor Performance Parameters. NASA TM X-73581, 1976.
5. Liebert, C. H.; and Stepka, F. S.: Potential Use of Ceramic Coating as a Thermal Insulation on Cooled Turbine Hardware. NASA TM X-3352, 1976.
6. Bill, R. C.: Plasma-Sprayed Zirconia Gas Path Seal Technology: A State-of-the-Art Review. NASA TM-79273, AVRADCOM TR 79-47, 1979.
7. Mularz, E. J.; Gleason, C. C.; and Dodds, W. J.: Combustor Concepts for Aircraft Gas Turbine Low-Power Emissions Reduction. NASA TM-78875, AVRADCOM TR-78-23(PL), 1978.
8. Stabe, R. G.; and Liebert, C. H.: Aerodynamic Performance of a Ceramic-Coated Core Turbine Vane Tested with Cold Air in a Two-Dimensional Cascade. NASA TM X-3191, 1975.
9. Ingham, H. S.; and Shepard, A. P.: Metco Flame Spray Handbook. Eighth ed. Metco, Inc., 1964.
10. McCullough, J. D.; and Trueblood, K. N.: The Crystal Structure of Baddeleyite (Monoclinic ZrO_2). Acta Crystallogra., vol. 12, 1959, pp. 507-511.
11. Mecartney, M. L.; Donlon, W. T.; and Heuer, A. H.: Plastic Deformation in CaO-Stabilized ZrO_2 (CSZ). J. Mater. Sci., vol. 15, 1980, pp. 1063-1065.
12. Kind, N. Y.; and Koshur, L. T.: High Temperature Refractory Materials based on Zirconia Stabilized by Rare Earth Oxides. Ogneupory no. 10, 1966, pp. 55-58.
13. Graves, G. A. Jr.,; Lynch, C. T.; and Mazdiyasni, K. S.: Preparation and Mechanical Properties of Hot-Pressed Zirconia-Zirconia Fabric Composites. Am. Ceram. Soc. Bull, vol. 49, no. 9, 1970 pp. 797-803.
14. Porter, D. L.; and Heuer, A. H.: Microstructural Development in MgO-Partially Stabilized Zirconia (Mg-PSZ). J. Am. Ceram. Soc., vol. 62, no. 5-6, May-June 1979, pp. 298-305.
15. Gupta, T. K.; Lange, F. L.; and Bechtold, J. H.: Effect of Stress-Induced Phase Transformation on the Properties of Polycrystalline Zirconia Containing Metastable Tetragonal Phase. J. Mater. Sci., vol. 13, 1978, pp. 1464-1470.
16. Cooke, R. G.; and Popper, P.: Thermal Cycling Behavior of Partially Stabilized Zirconia Ceramics. Special Ceramics 6, P. Popper, ed., British Ceramic Research Association, 1975, pp. 135-145.
17. Claussen, N.; and Ruhle, M.: Design of Transformation-Toughened Ceramics. The Science and Technology of Zirconia, A. H. Heuer and L. W. Hobbs, eds., American Ceramic Society, 1981, pp. 137-165.
18. Hannink, R. H. J.: Growth Morphology of the Tetragonal Phase in Partially Stabilized Zirconia. J. Mater. Sci., vol. 13, 1978, pp. 2487-2496.
19. Porter, D. L.; Evans, A. G.; and Heuer, A. H.: Transformation-Toughening in Partially-Stabilized Zirconia (PSZ). Acta Metall., vol. 27, 1979, pp. 1649-1654.
20. Garvie, R. C.: Stabilization of the Tetragonal Structure in Zirconia Microcrystals. J. Phys. Chem., vol. 82, no. 2, Jan. 26, 1978, pp. 218-224.
21. Lange, F. F.: Transformation Toughening - Part 3 Experimental Observations in the ZrO_2-Y_2O_3 System. J. Mater. Sci., vol. 17, 1982, pp. 240-246.

22. Miller, R. A.; Garlick, R. G.; and Smialek, J. L.: Phase Distributions in Plasma Sprayed Zirconia-Yttria. J. Amer. Cer. Soc., Dec. 1983.
23. Evans, A. G.; and Heuer, A. H.: REVIEW – Transformation Toughening in Ceramics: Martensitic Transformations in Crack-Tip Stress Fields. J. Am. Ceram. Soc., vol. 63, no. 5-6 May-June, 1980, pp. 241-248.
24. Lange, F. F.: Transformation Toughening (Parts 1-5). J. Mater. Sci., vol. 17, 1982, pp. 225-262.
25. Heuer, A. H.: Alloy Design in Partially Stabilized Zirconia. The Science and Technology of Zirconia, A. H. Heuer and L. W. Hobbs, eds., American Ceramic Society 1981, pp. 98-115.
26. Williamson, J., in the discussion section of reference 16.
27. Hannink, R. H. J.; and Garvie, R. C.: Sub-Eutectoid Aged Mg-PSZ Alloy with Enhanced Thermal Up-Shock Resistance. J. Mater. Sci., vol. 17, 1982, pp. 2637-2643.
28. Hannink, R. H. J.; et al.: Microstructural Changes during Isothermal Aging of a Calcia Partially Stabilized Zirconia Alloy. The Science and Technology of Zirconia, A. H. Heuer and L. W. Hobbs, eds., American Ceramic Society, 1981, pp. 116-136.
29. Porter, D. L.; and Heuer, A. H.: Mechanisms of Toughening Partially Stabilized Zirconia (PSZ). J. Am. Ceram. Soc., vol. 60, no. 3-4, Mar.-Apr. 1977, pp. 183-184.
30. Budiansky, B.; Hutchinson, J. W.; and Lambropovlos, J. C.: Continuum Theory of Dilatant Transformation Toughening in Ceramics. Int. J. Solids Struct., vol. 19, no. 4, 1983, pp. 337-355.
31. Ingel, R. P.; et al.: Temperature Dependence of Strength and Fracture Toughness of ZrO_2 Single Crystals. J. Am. Ceram. Soc., vol. 65, no. 9, Sept. 82, pp. C-150-C-152.
32. Pompe, W.; et al.: Increased Fracture Toughness of Brittle Materials by Microcracking in an Energy Dissipative Zone at a Crack Tip. J. Mater. Sci., vol. 13, 1978, pp. 2720-2723.
33. Valentine, Peter Glenn: Microstructure and Mechanical Properties of Bulk Yttria-Partially-Stabilized Zirconia. M. S. Thesis, Case Western Reserve Univ., 1982.
34. Rutman, D. S.; et al.: Vaporization of Components of Zirconia Ceramics. Ogneupory, vol. 33, no. 1, 1968, pp. 49-52.
35. Mitsuhashi, T.; Ichihara, M.; and Tatsuke, U.: Characterization and Stabilization of Metastable Tetragonal ZrO_2. J. Am. Ceram. Soc., vol. 57, no. 2, Feb. 1974, pp. 97-101.
36. Scott, H. G.: Phase Relationships in the Zirconia-Yttria System. J. Mater. Sci., vol. 10, 1975, pp. 1527-1535.
37. Stecura, S.: Two-Layer Thermal Barrier Coating for Turbine Airfoils-Furance and Burner Rig Test Results. NASA TM X-3425, 1976.
38. Miller, R. A.; Smialek, J. L.; and Garlick, R. G.: Phase Stability in Plasma-Sprayed Partially-Stabilized Zirconia-Yttria. The Science and Technology of Zirconia, A. H. Heuer and L. W. Hobbs, eds., American Ceramic Society 1981, pp. 241-253.
39. Kingery, W. D.; Bowen, H. K.; and Uhlmann, D. R.: Introduction to Ceramics, Second ed., John Wiley Sons, 1976.
40. Kittel, Charles: Introduction to Solid State Physics; Fifth ed. John Wiley Sons, 1976.
41. Touloukian, Y. S.; et al.: Thermophysical Properties of Matter, vol. 2, IFI/Plenum, 1970.
42. Garvie, R. C.: The Thermal Conductivity of Stabilized Zirconia. J. Mater. Sci., vol. 11, 1976, pp. 1365-1367.
43. Kingery, W. D. et al.: Thermal Conductivity: X, Data for Several Pure Oxide Materials Corrected to Zero Porosity. J. Am. Ceram. Soc., vol. 37, no. 2, Feb. 1954, pp. 107-110.
44. Mirkovich, V. V.: Comparative Method and Choice of Standards for Thermal Conductivity Determinations. J. Am. Ceram. Soc., vol. 48, no. 8, Aug. 21, 1965, pp. 387-391.
45. Ackerman, D. A.; et al.: Glass Behavior of Crystalline Solids at Low Temperatures. Phys. Rev., vol. B23, no. 8, April 15, 1981, pp. 3886-3893.
46. Liebert, C. H.: Emittance and Absorptance of NASA Ceramic Thermal Barrier Coating System-for turbine coaling. NASA TP-1190, 1978.
47. Liebert, C. H.; and Stepka, F. S.: Industry Tests of NASA Ceramic Thermal Barrier Coating. NASA TP-1425, 1979.
48. Taylor, C. M.: Thermal Stress Analysis of a Graded Zirconia/Metal Gas Path Seal System for Aircraft Gas Turbine Engines. NASA TM X-73658, 1977.
49. Wilkes, K. E.; and Lagedrost, J. F.: Thermophysical Properties of Plasma Sprayed Coating. (Battelle Columbus Labs; NAS3-13329.) NASA-CR-121144, 1973.
50. Boganov, A. G.; Pirogov, Y. A.; and Makarov, L. P.: Investigation of the Effective Thermal Conductivity and the Total Emmissivity of Heat-Resistant Ceramic Coatings of Refractory Oxides Produced by Gas-Flame Spraying. High Temp. (Engl. Transl.), vol. 3, 1965, pp. 53-58.
51. Gaffin, W. O.: JT9D Ceramic Outer Air Seal System Refinement Program. Pratt and Whitney Aircraft Group, (PWA-5515-165.) NASA CR-165554, 1982.
52. Terwilliger, G. R.; and Radford, K. C.: High Temperature Deformation of Ceramics: I, Background. Am. Ceram. Soc. Bull., vol. 53, no. 2, 1974, pp. 173-179; II, Specific Behavior, Am. Ceram, Soc. Bull., vol. 53, no. 6, 1974, pp. 465-472.
53. Von Mises, Z. Angew, Math. Mech. 62, 307 (1938) Quoted in reference 45.
54. Taylor, J. Inst. Met. 62, 307 (1938) Quoted in reference 45.
55. Hendricks, R. C.; McDonald, G.; and Mullen, R. L.: The Effect of Annealing on the Creep of Plasma Sprayed Ceramics. NASA TM-83396, 1983.
56. Phillips, D. S.; Mitchell, T. E.; and Heuer, A. H.: Precipitation in Star Sapphire III. Chemical Effects Accompanying Precipitation. Philos. Mag. A, vol. 42, no. 3, 1980, pp. 417-432.
57. Pletka, B.J.; Mitchell, T. E.; Heuer, A. H.: Solid Solution Hardening ofSapphire ($V-Al_2Q_3$). Phys. Status Solid A, vol. 39, 1977, pp. 301-311.
58. St: Jacques, R. G.; and Angers, R.: The Effect of CaO-Concentration on the Creep of CaO-Stabilized ZrO_2. Trans. Br. Ceram. Soc., vol. 72, no. 6, Sept. 1973, pp. 285-289.
59. Carter, R. E.; and Roth, W. L.: Conductivity and Structure in Calcia-Stabilized Zirconia. Electromative Force Measurements in High Temperature Systems, C. B. Alcock, ed., Institution of Mining and Metallurgy, 1968, pp. 125-144.
60. Schoenlein, L. H.; Hobbs, L. W.; and Heuer, A. H.: Precipitation and Ordering in Calcia- and Yttria-Stabilized Zirconia. J. Appl. Crystallogr., vol. 13, 1980, pp. 375-379.
61. Moghadam, F. K.; and Stevenson, D. A.: Influence of Annealing on the Electrical Conductivity of Polycrystalline $ZrO_2 + 8$ Wt% Y_2O_3. J. Am. Ceram. Soc., vol. 65, no. 4. April 1982, pp. 213-216.
62. Porter, D. L.: Microstructure-Mechanical Property Relationships in an MgO-Partially-Stabilized Zirconia. Ph.D. Thesis, Case Western Reserve University, 1977.
63. Notis, M. R.: Deformation Mechanism Maps-A Review with Applications. Deformation of Ceramic Materials, Richard Carl Bradt and R. E. Tressler, eds. Plenum Press, 1975, pp. 1-24.
64. Firestone, R. F.; Logan, W. R.; and Adams, J. W.: Creep of Plasma Sprayed Zirconia. (IIT Research Institute, IITRI-MO6071-20.) NAS-CR-167868, 1982.
65. Butler, E. P.; and Drennan, J.: Microstructural Analysis of Sintered High-Conductivity Zirconia with Al_2O_3 Additions. J. Am. Ceram. Soc., vol. 65, no. 10, Oct. 1982, pp. 474-478.

66. Rhodes, W. H.; and Carter, R. E.: Cationic Self-Diffusion in Calcia Stabilized Zirconia. J. Am. Ceram. Soc., vol. 49, no. 5, May 1966, pp. 244-249.
67. Simpson, L. A.; and Carter, R. E.: Oxygen Exchange and Diffusion in Calcia-Stabilized Zirconia. J. Am. Ceram. Soc., vol. 49, no. 3, Mar. 1966, pp. 139-144.
68. Smith, A. W.; Meszaros, F. W.; and Amata, C. D.: Permeability of Zirconia, Hafnia, and Thoria to Oxygen. J. Am. Ceram. Soc., vol. 49, no. 5, May 1966, pp. 240-244.
69. Kinergy, W. D.; et al.: Oxygen Ion Mobility in Cubic $Zr_{0.85}Ca_{0.15}O_{1.85}$. J. Am. Ceram. Soc., vol. 42, no. 8, Aug. 1959, pp. 393-398.
70. Oishi, Y.; Sakka, Y.; and Ando, K.: Cation Interdiffusion in Polycrystalline Fluorite-Cubic Solid Solutions. J. Nucl. Mater., vol. 96, no. 1-2, 1981, pp. 23-28.
71. Weast, J., ed.: Handbook of Chemistry and Physics. 53rd ed., Chemical Rubber Company, 1973.
72. Bill, R. C.; Sovey, J.; and Allen, G. P.: A Sputtered Zirconia Primer for Improved Thermal Shock Resistance of Plasma Sprayed Ceramic Turbine Seals. NASA TM-81732, AVRADCOM TR 81-C-6, 1981.
73. Zaplatynsky, I.: Reactions of Yttria-Stabilized Zirconia with Oxides and Sulfates of Various Elements. NASA TM-78942, 1978.
74. Wilson, H. H.: Destabilization of Zirconia by Phosphoric Acid. Am. Ceram. Soc. Bull., vol. 57, no. 4, 1978, pp. 455.
75. Taimatsu, H.; et al.: Reactions Between Stabilized Zirconia for Oxygen Sensor and Iron Oxides. Nippon Kinzoku Gakkaishi, vol. 46, no. 5, 1982, pp. 480-486.
76. Hodge, P. E.; Miller, R. A.; and Gedwill, M. A.: Evaluation of Hot Corrosion Behavior of Thermal Barrier Coatings. NASA TM-81520, 1980.
77. Siemers, P. A.; and McKee, P. A.: Investigations of Modified Zirconia Thermal Barrier Coatings for Gas-Turbine Applications. DOE/ET/11289-T8, General Electric Co., 1980.
78. G. Rozak and J. W. Halloran, "Reactions Between Y_2O_3, ZrO_2 and SiC or Si_3N_4 Structural Ceramics," NASA Grant No. NAG3-282, June-Sept. 1981.
79. Trigg, M. B.; and McCartney, E. R.: Comparison of the Reaction Systems ZrO_2-Si_3N_4 and TiO_2-Si_3N_4. J. Am. Ceram. Soc., vol. 64, Nov. 1981, pp. C-151-C-152.
80. LeFevre, J.: Some Structural Modification of Fluorite-type Phases In Systems Based on Zirconia or Hafnium Oxide. Ann. Chim. (Paris), vol. 8, no. 1-2, 1963, pp. 117-149.
81. Bailey, J. E.: The Monoclinic-Tetragonal Transformation and Associated Twinning in Thin Films of Zirconia. Proc. R. Soc., London, Ser. A, vol. 279A, no. 1378, June 9, 1964, pp. 395-412.
82. Grain, C. F.: Phase Relations in the ZrO_2-MgO System. J. Am. Ceram. Soc., vol. 50, no. 6, June 1967, pp. 288-290.
83. Stubican, V. S.; Hink, R. C.; and Ray, S. P.: Phase Equilibria and Ordering in the System ZrO_2-Y_2O_3. J. Am. Ceram. Soc., vol. 61, no. 1-2, Jan-Feb, 1978, pp. 17-21.
84. Matlock, D. K., and Nix, W. D.: The Effect of Sample Size on the Steady State Creep Characteristics of Ni-6 pct W., Met. Trans, vol. 5, 1974, pp. 1401.
85. Norton, F. H.; et al.: Progress Report for July 1-September 30, 1950. NYO-596, 1950.
86. Fitzsimmons, E. S.: Basic Material Studies: Compressive Creed and Fracture Properties of Be O Composites. APEX-686, General Electric Co., July 1961.

1. Report No.	2. Government Accession No.	3. Recipient's Catalog No.
NASA TP-2286		

4. Title and Subtitle	5. Report Date
Overview of Zirconia With Respect to Gas Turbine Applications	March 1984
	6. Performing Organization Code: 505-33-52

7. Author(s)	8. Performing Organization Report No.
James D. Cawley	E-1726
	10. Work Unit No.

9. Performing Organization Name and Address	11. Contract or Grant No.
National Aeronautics and Space Administration Lewis Research Center Cleveland, Ohio 44135	
	13. Type of Report and Period Covered: Technical Paper

12. Sponsoring Agency Name and Address	14. Sponsoring Agency Code
National Aeronautics and Space Administration Washington, D.C. 20546	

15. Supplementary Notes

16. Abstract

A review is made of the literature on zirconia, with an emphasis on material properties, referenced to its application in gas turbine engines. The review indicates that Mg-PSZ (partially stabilized zirconia) and Ca-PSZ are unsuitable for advanced gas turbine applications; a thorough characterization of the microstructure of plasma-sprayed zirconia is needed. Transformation-toughened zirconia may be suitable for use in monolithic components.

17. Key Words (Suggested by Author(s))	18. Distribution Statement
Zirconia Material properties Plasma-sprayed zirconia Overview	Unclassified - unlimited STAR Category 27

19. Security Classif. (of this report)	20. Security Classif. (of this page)	21. No. of pages	22. Price*
Unclassified	Unclassified	28	A03

*For sale by the National Technical Information Service, Springfield, Virginia 22161

NASA-Langley, 198

2 2 1U,C, 840315 S00161DS
DEPT OF THE AIR FORCE
ARNOLD ENG DEVELOPMENT CENTER(AFSC)
ATTN: LIBRARY/DOCUMENTS
ARNOLD AF STA TN 37389